

Scuola di Scienze
Dipartimento di Fisica e Astronomia
Corso di Laurea Magistrale in Fisica

**ELECTROSPUN NANOFIBERS FOR
ELECTROMECHANICAL TRANSDUCTION
INVESTIGATED BY SCANNING PROBE
MICROSCOPY**

Relatore:
Prof. Beatrice Fraboni

Presentata da:
Francesco Calavalle

Correlatore:
Dott. Tobias Cramer

Sommario

Electrospun nanofibers for electromechanical transduction investigated by Scanning Probe Microscopy

Francesco CALAVALLE

Negli ultimi anni, il copolimero ferroelettrico P(VDF-TrFE), ha suscitato un grande interesse nella ricerca scientifica per le potenziali applicazioni elettroniche come ad esempio l'energy harvesting per la produzione di dispositivi indossabili e autoalimentabili, sensori biocompatibili e memorie non volatili. Molti sforzi si sono concentrati nello sviluppo di procedure di fabbricazione che possano migliorare le performance elettromeccaniche di questi materiali. Una delle soluzioni proposte è un processo chiamato elettrofilatura, una tecnica efficiente e a basso costo che sarebbe in grado di realizzare nanofibre polimeriche già polarizzate e pronte per l'integrazione nei dispositivi.

Dalle analisi microscopiche svolte in questa tesi, utilizzando tecniche di microscopia a scansione di sonda, è stato scoperto che in realtà l'elettrofilatura non provoca polarizzazione nelle fibre, bensì induce un processo di iniezione di cariche all'interno del materiale che, se testato a livello macroscopico, mostra un'apparente risposta ferroelettrica dovuta però alle cariche intrappolate, come in un elettreto. Nonostante ciò, dopo la dissipazione delle cariche spaziali, ho potuto dimostrare, grazie all'implementazione della Switching Spectroscopy PFM ad alto potenziale, che le nanofibre elettrofilate possono essere polarizzate e mostrano proprietà piezoelettriche simili a quelle del film sottile. Quindi, inducendo la completa polarizzazione del network dopo la deposizione, è auspicabile un miglioramento delle proprietà elettromeccaniche dei dispositivi basati su nano-fibre elettrofilate.

Abstract

Electrospun nanofibers for electromechanical transduction investigated by Scanning Probe Microscopy

Francesco CALAVALLE

The ferroelectric copolymer P(VDF-TrFE), has attracted, in recent years, a great interest in scientific research for modern electronics applications, such as energy harvesting for self-powered wearable devices, biomedical sensors and nonvolatile memories. Lots of efforts have been spent in the development of fabrication procedures that could enhance the electromechanical performance of this material. Electrospinning has been proposed as an efficient and low-cost solution for the production of polarized polymeric nanofibers, ready for the integration in devices without post-poling process required.

In this thesis, I employ Scanning Probe Microscopy techniques to provide an accurate investigation of the electromechanical properties of single P(VDF-TrFE) electrospun nanofibers. I find that electrospinning does not induce ferroelectric polarization of the fibers, but leads to the accumulation of space charges in the material. I argue that such a space charge gives rise to an apparent ferroelectric response at the macroscopical scale due to the electret effect. Further, after dissipation of the space-charges, with the implementation of high voltage Switching Spectroscopy-PFM, I could demonstrate that poling processes at the level of a single nano-fiber are possible and that the observed piezoelectric performance is comparable to the thin-film behavior. Therefore, I predict that electrospun fibers will show improved behavior in electromechanical devices once complete poling of fiber networks is achieved.

Contents

| | |
|---|------------|
| Sommario | iii |
| Abstract | v |
| Introduction | 1 |
| 1 Piezo- and Ferroelectric polymers in electronic applications | 3 |
| 1.1 Background | 4 |
| 1.1.1 Dielectric materials | 4 |
| 1.1.2 Electric Polarization | 5 |
| 1.1.3 Electrostrictive effect | 6 |
| 1.2 Theory of Piezo- and Ferroelectric effect | 7 |
| 1.2.1 Piezoelectricity | 7 |
| Piezoelectric Coupling Coefficient k | 12 |
| 1.2.2 Ferroelectricity | 12 |
| Phase transitions | 13 |
| Ferroelectric hysteresis Loop | 14 |
| 1.3 Electrets | 16 |
| 1.3.1 Charge formation in electrets | 17 |
| Two-Charge Theory | 17 |
| 1.4 Piezo- and Ferroelectric polymers | 18 |
| 1.4.1 PVDF | 19 |
| 1.4.2 P(VDF-TrFE) | 20 |
| 1.5 Applications | 21 |
| 1.5.1 Energy harvesting devices | 22 |
| 1.5.2 Nonvolatile Memories | 23 |
| 1.5.3 Other Applications | 24 |
| Negative Capacitance devices | 25 |
| Photovoltaic devices | 25 |
| Sensors and actuators | 26 |

| | | |
|----------|--|-----------|
| 2 | Fabrication Methods | 27 |
| 2.1 | Thin film preparation | 27 |
| 2.2 | Electrospun Nanofibers | 28 |
| 2.2.1 | Electrospinning | 28 |
| | Operational parameters | 30 |
| 2.2.2 | P(VDF-TrFE) nanofibers | 32 |
| 3 | Scanning Probe Microscopy techniques | 33 |
| 3.1 | Piezoresponce Force Microscopy (PFM) | 33 |
| 3.1.1 | Experimental Setup | 34 |
| 3.1.2 | Elementary theory and applications of PFM | 35 |
| | Analysis of First Harmonic Signal | 39 |
| 3.1.3 | Calibration of the piezoresponse signal | 40 |
| 3.2 | Kelvin Probe Force Microscopy (KPFM) | 41 |
| 3.2.1 | Basic principles of non-contact AFM | 42 |
| 3.2.2 | Fundamentals of KPFM | 43 |
| 4 | Results and Discussions | 47 |
| 4.1 | Implementation of SS-PFM | 47 |
| 4.2 | PFM on P(VDF-TrFE) thin film | 51 |
| 4.3 | PFM on P(VDF-TrFE) nanofibers | 57 |
| 4.4 | Charging effects in electrospun P(VDF-TrFE) nanofibers | 61 |
| 4.4.1 | Effects of Polarization Switching on Surface Potential | 64 |
| | Conclusions | 67 |

Introduction

An emerging direction in technological progress leads to the rapid growth of mobile and portable electronics for applications in communication, personal health care, and environmental monitoring. The integration of energy harvesting systems, capable of producing energy from waste sources, is of great interest in order to project self-sustainable, wearable devices. Developments in materials science, mechanics and manufacturing now enable the construction of thin and flexible piezoelectric systems for powering electronic devices [1]. Among the wide range of piezoelectric materials, semicrystalline polymers revealed to be easily tailored at the nanoscale to achieve non-toxic, low-temperature, and relatively low-cost processing structures with a high flexibility, light weight, and easy deformation properties. For all these advantages, they have recently raised great interest in the scientific community, offering new and promising solutions for the fabrication of polymer-based devices.

In recent years, intensive research efforts has been made on the studies of new organic devices based on polyvinylidene fluoride (PVDF) and its copolymer with trifluoroethylene (TrFE), which are the most representative organic ferroelectric, and thus piezoelectric, materials. The FE/PE properties of these polymers arise due to the molecular dipoles present in the monomer unit ($\text{CH}_2\text{-CF}_2$) that are aligned perpendicular to the main chain axis [2]. Because of the ferroelectric properties, P(VDF-TrFE) is not only attractive for electromechanical application, but it is also promising candidate for the next generation nonvolatile high-density memory applications which can replace perovskite ceramics currently used in the commercial ferroelectric random access memories (FRAMs) [3, 4]. Furthermore, due to their biocompatibility, these polymers are suitable for biomedical application such as implantable sensors [5]. Despite the great advantages described, generally, P(VDF-TrFE) presents lower performance compared to more traditional ceramic FE/PE materials such as PZT and BTO [6].

Preparation process optimizations, and dimension lowering strategies have presented from previous work as the most effective way to improve the performance of polymer-based devices. Nanostructured materials, exhibit new physical phenomena

because of finite size effects that occur during down-scaling [7, 8]. Electrospinning is one of the technique proposed for the low-cost production of nanofibers from polymeric solutions. It has been suggested that this method can give rise to preferentially oriented induced dipoles in P(VDF-TrFE) nanofibers with a single stage process [9].

Although, some improvements in performance of devices with integrated P(VDF-TrFE) electrospun nanofibers has been observed, it is not clear what relationship there is between the fabrication method and the microscopic effects on properties of P(VDF-TrFE).

The objective of this thesis is to investigate the effect brought by electrospinning process on ferroelectric and piezoelectric properties of P(VDF-TrFE) at the nanometer scale, using Scanning Probe Microscopy techniques.

Chapter 1, starts with a wide introduction on the origin and the theory behind ferroelectricity and piezoelectricity in dielectric materials. In addition, the structure and the main properties, as well as the most attractive applications of P(VDF-TrFE) are presented.

P(VDF-TrFE) thin film and electrospun nanofibers samples, analysed in this work, are described together with the respectively fabrication methods in Chapter 2.

The next Chapter provides to explain PFM (Piezoresponse Force Microscopy) and KPFM (Kelvin Probe Force Microscopy), the two SPM techniques used to perform measurements on the samples. These methods of investigation are fundamental for the purpose of my work, since they allow the acquisition of information about piezoelectric response and surface potential of the samples with an extraordinary spatial resolution.

In Chapter 4, the results collected by the experiments designed during this work are described and discussed. The Chapter starts with the description of the setup implemented for Switching Spectroscopy PFM measurements. In the central part, the results obtained from PFM measurements on P(VDF-TrFE) thin film and electrospun nanofibers are compared. Finally, surface potential measurements are reported to explain the charging process induced by electrospinning.

Chapter 1

Piezo- and Ferroelectric polymers in electronic applications

Piezoelectricity was observed for the first time in 1880 by French physicists Jacques and Pierre Curie. A subset of piezoelectricity is ferroelectricity, so all ferroelectric materials are piezoelectric (Figure 1.1). The term ferroelectricity arise by analogy with ferromagnetism, mainly because they have similar characteristics respectively related to electric and magnetic field. The prefix *piezo-* in the word piezoelectrics instead is derived from a Greek word, *piezein*, meaning pressure. Piezoelectrics are materials in which electricity can be generated by an applied mechanical stress or a mechanical stress can be produced by an applied electric field. The term piezoelectricity has been used by scientists since 1881 to distinguish the piezoelectric phenomena from electrostriction. Piezo- and ferroelectric materials exhibit interesting electromechanical properties that have led to interesting applications. There is, therefore, a need to have a basic understanding of piezo- and ferroelectric materials as well as the relationship between them when developing piezoelectric-based energy harvesting systems, ferroelectric memories or other sensing application.[10]

The aims of this chapter is to give the reader a basic introduction to the underlying physics and principles of piezo- and ferroelectric materials. These are materials that have been well known and described since the late 1800s and as such there is significant historical knowledge and understanding to be drawn upon. Furthermore, it will be described a wide range of application in modern electronics, such as energy harvesting and nonvolatile memory.

1.1 Background

1.1.1 Dielectric materials

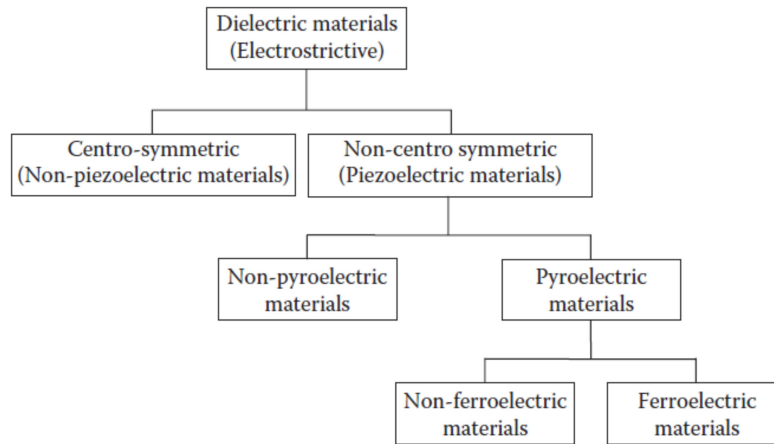


FIGURE 1.1: Relationship between crystal classes and piezo-,pyro- and ferroelectric properties [11].

In general, piezo- and ferroelectric materials are first of all dielectrics, in fact the characteristic properties of these materials are strongly related to the polarization induced by external electric fields or other stimuli like mechanical stress. All dielectric materials when subjected to an external electric field exhibit a displacement of cations and anions respectively in the same and opposite direction of the applied field, resulting in a net deformation of the material. The degree of deformation depends on crystal class to which the dielectric belongs. Of the 32 crystal classes, 11 are centrosymmetric (i.e., possess a centre of symmetry or inversion centre) and 21 are noncentrosymmetric (do not possess a centre of symmetry) [11]. When a dielectric material possessing a centre of symmetry is subjected to an external electric field, due to the symmetry (inversion centre), the movements of cations and anions are such that the extension and contraction get cancelled between neighbouring chemical bonds and the net deformation in the crystal is ideally nil. But the chemical bonds are not perfectly harmonic and, due to the anharmonicity of the bonds, there will be second-order effects resulting in a small net deformation of the lattice. This effect is called electrostrictive effect and exists in all dielectrics caused by the anharmonicity of chemical bonds. When a dielectric material belonging to a noncentrosymmetric class (except the octahedral class)

is subjected to an external electric field, there will be asymmetric movement of the neighbouring ions, resulting in significant deformation of the crystal and the deformation is directly proportional to the applied electric field. These materials exhibit an electrostrictive effect due to the anharmonicity of the bonds, but it is masked by the more significant asymmetric displacement. These materials are called piezoelectric materials [11]. The classification of dielectric materials based on their response to external stimuli is shown in Figure 1.1.

1.1.2 Electric Polarization

In an atom or a molecule when the centres of positive and negative charges are separated by a certain distance d , the atom or the molecule possesses an electric dipole moment given by

$$\mathbf{p} = q\mathbf{d}, \quad (1.1)$$

where q is the charge, \mathbf{d} is the separation between the positive and negative charge centres and \mathbf{p} is a vector with direction from negative to positive charge. Dielectric materials may be classified as polar and nonpolar. In nonpolar dielectric materials, normally the atoms do not possess an electric dipole moment as the centres of positive and negative charges coincide. When these materials are subjected to an external electric field, the centres of positive and negative charges get separated and thus dipole moments are induced until the field is applied. In polar dielectric materials, each atom or molecule possesses a dipole moment as the centres of positive and negative charges do not coincide, so when an external electric field is applied to these materials, the electric dipoles tend to orient themselves in the direction of the field. Examples of polar and nonpolar materials are respectively H_2O and O_2 [11].

A polar dielectric material consists of a large number of atoms or molecules each possessing an electric dipole moment. Electric polarization \mathbf{P} is defined as the total dipole moment per unit volume and is given by

$$\mathbf{P} = \frac{\sum_i \mathbf{p}_i}{V}, \quad (1.2)$$

where V is the volume of the material. \mathbf{P} is a vector normal to the surface of the material, and it is sometimes called the surface charge density. In general, in a polar dielectric, the individual electric dipoles are all randomly oriented and so the

net polarization is zero. When an electric field \mathbf{E} is applied, the material develops a finite polarization that increases as the field increase, reaching saturation when all the dipole moments are oriented in the direction of the field.

The displacement field \mathbf{D} developed inside the material due to the external field is given by

$$\mathbf{D} = \epsilon_0 \mathbf{E} + \mathbf{P}, \quad (1.3)$$

where ϵ_0 is the permittivity of free space. \mathbf{D} is also expressed by the relation

$$\mathbf{D} = \epsilon \mathbf{E} = \epsilon_0 \epsilon_r \mathbf{E}, \quad (1.4)$$

where ϵ_r is the relative permittivity or dielectric constant of the dielectric material. The polarization \mathbf{P} is directly related to \mathbf{E} by the relation

$$\mathbf{P} = \epsilon_0 \chi \mathbf{E}, \quad (1.5)$$

where χ is called the electric susceptibility of the material [11]. From Equations 1.3, 1.4 and 1.5, we get the relation between the dielectric constant and electric susceptibility as

$$\epsilon_r = 1 + \chi. \quad (1.6)$$

1.1.3 Electrostrictive effect

Electrostriction is a basic electromechanical phenomenon that occurs in all insulators or dielectrics. It is present in all crystal symmetries because is a fourth rank polar tensor. Electrostriction is a measure of the polarization induced by ions shifting away from their natural equilibrium positions, giving rise to variations in the lattice parameters (strain). In centrosymmetric crystals, the induced shifts of equivalent ions almost cancel each other out, while the difference in the shifts because of potential anharmonicity generates strain. The induced strain (S_{ij}) is proportional to the square of electric field (E_i)/polarization (P_i), and it can be expressed in the following equations:

$$\begin{aligned} S_{ij} &= Q_{ijkl} P_k P_l, \\ S_{ij} &= M_{ijkl} E_k E_l, \end{aligned} \quad (1.7)$$

where Q_{ijkl} and M_{ijkl} are electrostrictive coefficients.

The strain induced by the electrostrictive effect is generally small when compared with that induced by piezoelectricity. Consequently, there has been limited attention focusing on the electrostrictive effect. In the 1980s, a systematic study on electrostriction was carried out on relaxor ferroelectrics with perovskite structures in which a high electrostrictive strain was observed because of the high dielectric response of the relaxors [12]. In addition, in the 1990s, investigations on electrostriction were performed on polymers, including ferroelectric polymers, dielectric elastomers, and polymer composites. Ultra-high electrostrictive strains were observed in these polymeric materials (>4% for polyvinylidene fluoride [PVDF] and >40% for silicone), giving them potential for use in actuator applications [13]. On the other hand, ferroelectrics are the mainstay materials for piezoelectric transducer and actuator applications and have been reported to possess much higher piezoelectric responses when compared with non-ferroelectric materials [14]. The electrostrictive effect plays a key role in the electromechanical behavior in ferroelectrics, investigations on which will benefit the exploration of high-performance piezoelectrics [15].

1.2 Theory of Piezo- and Ferroelectric effect

1.2.1 Piezoelectricity

Dielectric materials that belong to the class of noncentrosymmetric crystals (Figure 1.2) are classified as piezoelectric materials. There's a lot of materials that exhibit piezoelectricity, for examples natural like Quartz and Lead titanate (PbTiO_3) and synthetic ones like quartz like crystals, perovskite ceramics and also polymers. To achieve the piezoelectric properties usually these materials are subjected to a "poling process" in order to align the domains of polarization in a preferential direction.

When these materials are subjected to external strain by applying a mechanical sollecitation like strain or pressure, the electric dipoles in the crystal get oriented such that the crystal develops positive and negative charges on opposite faces, resulting in an electric field across the crystal. This is called direct piezoelectric effect. An interesting feature of this phenomenon is the reversibility, in fact in the opposite situation the application of an external electric field, will result in an asymmetric displacements of anions and cations that cause considerable net deformation of

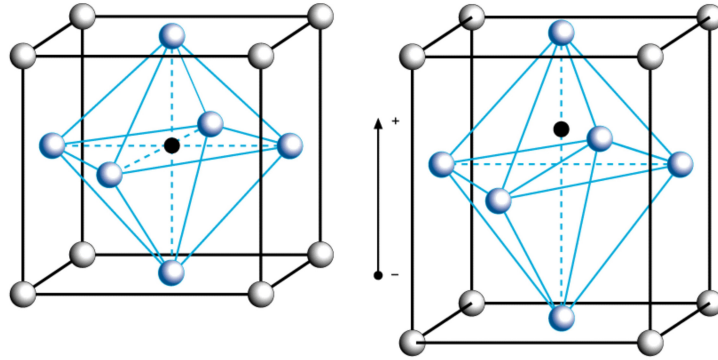


FIGURE 1.2: Typical crystal structure of a piezoelectric perovskite, before and after polarization [16].

the crystal. This is known as the indirect piezoelectric effect. The relation between strain and applied electric field is, in first approximation linear, unlike for electrostrictive materials in which the strain is proportional to E^2 . The strain in a piezoelectric material is extensive or compressive, depending on the polarity of the applied field. The direct and indirect piezoelectric effects are illustrated in Figure 1.3. In the direct effect when a poled piezoelectric material is subjected to tensile stress, in the direction parallel to the poling direction, a positive voltage is generated across the faces. When the stress is compressive in the same direction, a negative voltage is generated across the faces. In the indirect effect, when an external voltage is applied to the material, the material gets extended if the polarity of the voltage is the same as that of the field applied during poling and, when the voltage is applied in the reverse direction, the material gets compressed. The reaction generated by the applied stimulus in both case is barely instantaneous, so the application of external alternating fields produces alternate compression and extension at the same frequency of the electric field.

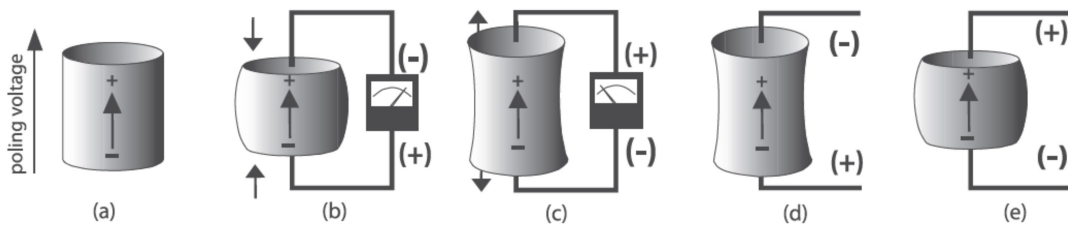


FIGURE 1.3: Schematic representation of direct and inverse piezoelectric effect [17].

Now let's introduce the equations which describe electromechanical properties of piezoelectric materials. In this formulation it's been assumed that piezoelectric materials are linear, this is a good approximation at low electric fields and at low mechanical stress levels. However, they may show considerable nonlinearity if operated under a high electric field or high mechanical stress level. A tensor notation is adopted to identify the coupling between the various entities through the mechanical and electrical coefficients. The common practice is to label directions as depicted in Figure 1.4, so with 1, 2, 3 to indicate x, y, z and 4, 5, 6 to indicate the shear planes perpendicular to the respective axis.

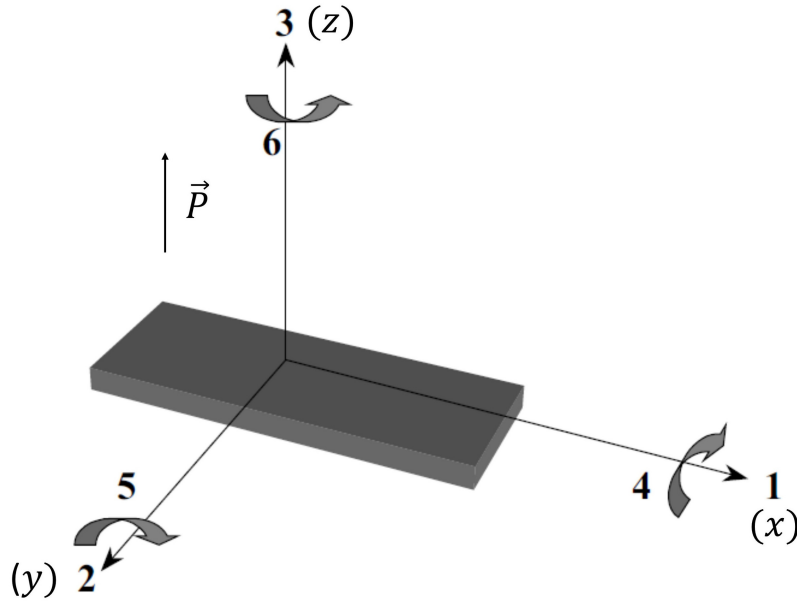


FIGURE 1.4: Tensor direction for defining constitutive equation [18].

Piezoelectricity can be described as a coupling between behaviour of elastic variables, stress T and strain S , and dielectric variables, displacement of charge density D and applied electric field E . Combining Equation 1.4 and the Hook's Law:

$$\mathbf{S} = s\mathbf{T}, \quad (1.8)$$

where s is the compliance, one can obtain the electromechanical equations for a linear piezoelectric material:

$$S_i = s_{ij}^E T_j + d_{mi} E_m, \quad (1.9)$$

$$D_m = d_{mi} T_i + \epsilon_{ik}^T E_k, \quad (1.10)$$

where the index $i, j = 1, 2, 3, 4, 5, 6$ and $m, k = 1, 2, 3$ refer to different directions within the material coordinate system, d is the matrix of piezoelectric constants, ϵ is the dielectric permittivity and the superscripts T and E indicates constant electric field and stress field across the system [17]. There a total of four piezoelectric coefficients, d_{ij} , e_{ij} , g_{ij} , h_{ij} , all related to each other through electrical and mechanical properties of the material and by convention are defined as follows:

$$d_{ij} = \left(\frac{\partial D_i}{\partial T_j} \right)^E = \left(\frac{\partial S_j}{\partial E_i} \right)^T, \quad (1.11)$$

$$e_{ij} = \left(\frac{\partial D_i}{\partial S_j} \right)^E = \left(\frac{\partial T_j}{\partial E_i} \right)^S, \quad (1.12)$$

$$g_{ij} = \left(\frac{\partial E_i}{\partial T_j} \right)^D = \left(\frac{\partial S_j}{\partial D_i} \right)^T, \quad (1.13)$$

$$h_{ij} = \left(\frac{\partial E_i}{\partial S_j} \right)^D = \left(\frac{\partial T_j}{\partial D_i} \right)^S. \quad (1.14)$$

In each Equation above the right terms are related to the direct effect and the left ones to the inverse effect; d_{ij} represent the piezoelectric strain constants, e_{ij} the stress constants, g_{ij} the piezoelectric voltage constants and h_{ij} the strain constants [18]. Equations 1.9, 1.10 could have been written in the matrix form applying some simplifications. In fact if one assumes the device or material transversely isotropic and that it's poled along one axis (for example axis 3), many of the parameters in matrix will be either zero or can be express in terms of other parameters. Rewriting those equations in matrix form one obtains the following expression:

$$\begin{bmatrix} S_1 \\ S_2 \\ S_3 \\ S_4 \\ S_5 \\ S_6 \end{bmatrix} = \begin{bmatrix} s_{11} & s_{12} & s_{13} & 0 & 0 & 0 \\ s_{12} & s_{11} & s_{13} & 0 & 0 & 0 \\ s_{13} & s_{13} & s_{33} & 0 & 0 & 0 \\ 0 & 0 & 0 & s_{44} & 0 & 0 \\ 0 & 0 & 0 & 0 & s_{44} & 0 \\ 0 & 0 & 0 & 0 & 0 & 2(s_{11} - s_{12}) \end{bmatrix} \begin{bmatrix} T_1 \\ T_2 \\ T_3 \\ T_4 \\ T_5 \\ T_6 \end{bmatrix} + \begin{bmatrix} 0 & 0 & d_{31} \\ 0 & 0 & d_{31} \\ 0 & 0 & d_{33} \\ 0 & d_{15} & 0 \\ d_{15} & 0 & 0 \\ 0 & 0 & 0 \end{bmatrix} \begin{bmatrix} E_1 \\ E_2 \\ E_3 \end{bmatrix}, \quad (1.15)$$

and

$$\begin{bmatrix} D_1 \\ D_2 \\ D_3 \end{bmatrix} = \begin{bmatrix} 0 & 0 & 0 & 0 & d_{15} & 0 \\ 0 & 0 & 0 & d_{15} & 0 & 0 \\ d_{31} & d_{31} & d_{33} & 0 & 0 & 0 \end{bmatrix} \begin{bmatrix} T_1 \\ T_2 \\ T_3 \\ T_4 \\ T_5 \\ T_6 \end{bmatrix} + \begin{bmatrix} \epsilon_{11}^T & 0 & 0 \\ 0 & \epsilon_{11}^T & 0 \\ 0 & 0 & \epsilon_{33}^T \end{bmatrix} \begin{bmatrix} E_1 \\ E_2 \\ E_3 \end{bmatrix}. \quad (1.16)$$

The ‘‘piezoelectric strain constant’’ d is defined as the ratio of developed free strain to the applied electric field. The subscript d_{ij} implies that the electric field is applied or charge is collected in the i direction for a displacement or force in the j direction. In order to give a physical explanation of the d coefficient let’s consider a device made of two electrodes connected to opposite sides of a piece of piezoelectric material poled in direction 3 of thickness t , length l and width w . If a voltage V is applied to this transducer this voltage generates the electric field:

$$E_3 = \frac{V}{t}, \quad (1.17)$$

which strains the transducer in different directions. In particular

$$S_1 = \frac{\Delta l}{l}, \quad (1.18)$$

in which

$$\Delta l = \frac{d_{31} V l}{t}. \quad (1.19)$$

The piezoelectric constant d_{31} is usually a negative number. This is due to the fact that application of a positive electric field will generate a positive strain in direction 3. Another interpretation of d_{ij} is the ratio of short circuit charge per unit area flowing between connected electrodes perpendicular to the j direction to the stress applied in the i direction. If a force F is applied to the transducer, in the 3 direction, it generates the stress

$$T_3 = \frac{F}{lw}, \quad (1.20)$$

which results in the electric charge

$$q = d_{33}F, \quad (1.21)$$

flowing through the short circuit [17]. The other coefficients are of less interest for the goal of this work but they can be treated with analogous considerations and they give other relationship between electromechanical properties.

Piezoelectric Coupling Coefficient k

Piezoelectric coupling coefficient is a measure of the efficiency of a piezoelectric material as a transducer. It quantifies the ability of the piezoelectric material to convert one form of energy (mechanical or electrical) to the other form (electrical or mechanical). If one define the mechanical work made by an applied force W_M as

$$W_M = \frac{F\Delta z}{2}, \quad (1.22)$$

and the electrical energy W_E generated by the displacement of charge due to the piezoelectric effect

$$W_E = \frac{Q^2}{2C_p}, \quad (1.23)$$

which is the energy stored in the piezoelectric capacitor. If one consider directions parallel to the polarization the piezoelectric coupling will be

$$k_{33} = \sqrt{\frac{W_E}{W_M}} = \frac{Q}{\sqrt{F\Delta z C_p}}. \quad (1.24)$$

In general this coefficient can be written in terms of other parameters and direction, in particular as

$$k_{ij}^2 = \frac{d_{ij}^2}{s_{ij}^E \epsilon_{ij}^T}. \quad (1.25)$$

1.2.2 Ferroelectricity

Ferroelectric materials are a subclass of piezoelectric materials. Thus, they exhibit piezoelectric properties and also they have more sensitive characteristics, so most of the practical piezoelectric devices use ferroelectric materials. Ferroelectric materials exhibit spontaneous polarization but they have the characteristic property that allows an inversion of this polarization with the application of an external electric

field. another feature of ferroelectrics is that the polarization \mathbf{P} as a function of the applied electric field \mathbf{E} is nonlinear. The main properties of ferroelectric materials are the following:

- Ferroelectric hysteresis;
- Spontaneous polarization;
- Reversible polarization;
- Ferroelectric phase transition temperature.

The description of the arrangement of polarization in a ferroelectric material uses a domain structure similar to the structure used in ferromagnetic materials. Ferroelectric domain is defined as a small microscopic region in the material within which all the electric dipoles are oriented in the same direction due to a strong short-range interaction caused by internal electric fields. This preferential direction of polarization is present within the domains even without applied electric field and it is called spontaneous polarization. Ferroelectric materials are made of a large number of domains, each one with a spontaneous polarization in a specific direction. Normally, the domains are all randomly oriented, and so the net polarization of the material is zero in the absence of an external electric field. When an external electric field is applied, the domains tend to get oriented in the direction of the applied field. The process that regulate this reorientation consists of the growing in size of domains that are in the direction of the external field at the expense of the other domains. As the external field is increased, more and more domains get oriented in the direction and ultimately the material ideally consists of a single domain [11].

Phase transitions

The properties of ferroelectrics can be understood by reference to a fictitious one-dimensional crystal made up of two atoms of opposite charge. In this crystal, it is clear that we can orient the dipoles to point all to the right, or all to the left. The two structures are completely equivalent, except that they have an opposite sign to the dipole moment. They must therefore have exactly the same energy. We could transform one into the other by dragging one type of atom toward the other. As we do this, the bulk polarisation will reduce in magnitude, and change

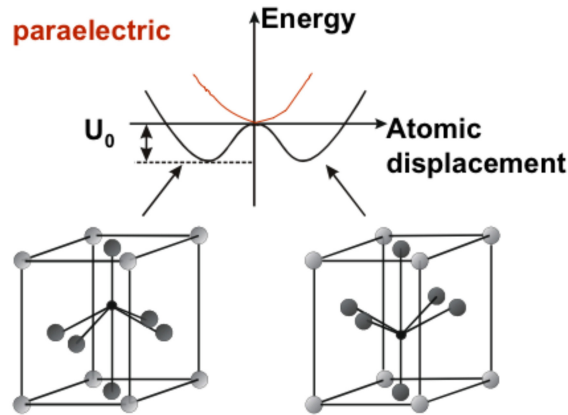


FIGURE 1.5: Schematic potential wells and crystal configuration of two ferroelectric states [19].

sign at the point where the atoms are equally spaced and finally switch to the opposite direction. Given that we know the crystal is stable in either of the two polarised states, there must be an energy barrier between the two states, and we can sketch a curve (Figure 1.5) for the energy as a function of the polarisation. It is common to observe that as the temperature is raised, the bulk polarisation decreases and vanishes abruptly at a temperature T_c . This is a phase transition, just as in a ferromagnet raised above its Curie temperature, or a solid raised above its melting point. It arises microscopically because as temperature is raised the thermal vibrations of the atoms in the solid cause fluctuations which overcome the potential barrier between the two (or more) wells.

The detailed microscopic theory of phase transition will be different from material to material, but the macroscopic properties will be similar across many classes of materials and they can be described with the Landau theory of phase transitions [20].

Ferroelectric hysteresis Loop

The application of an external electric field to switch polarization in a ferroelectric material leads to the characteristic hysteresis loop of \mathbf{P} vs \mathbf{E} . With the application of an electric field \mathbf{E} the two stable states no longer have the same energy because of the electric polarisation energy $-\mathbf{P} \cdot \mathbf{E}$, so the wells are tilted by the electric field. It is also clear from Figure 1.6 that a small field will not necessarily immediately switch the polarisation from one direction to the other because there is a barrier to be overcome.

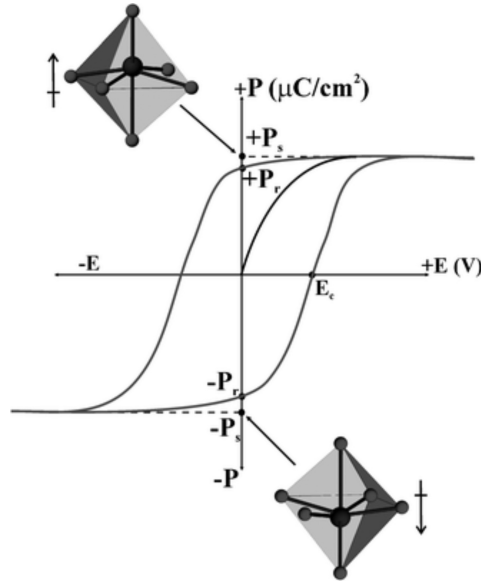


FIGURE 1.6: Typical hysteresis loop of a ferroelectric material.

Initially, when the applied field is zero, the ferroelectric domains are all randomly oriented and so the polarization is zero. As the field is increased, the domains get oriented in the direction of the field, and the polarization increases linearly in the beginning. As the field is further increased, more and more domains get oriented, the curve becomes nonlinear, and ultimately when all the domains get oriented, the polarization attains the maximum value P_S called saturation polarization. If the electric field is now reduced gradually, the polarization decreases but the curve is not retraced. The decrease in polarization is rather slow because of the barrier for the reorientation of domains and the polarization lags behind the electric field. When the field is reduced to zero, there remains a finite polarization called the remnant polarization P_R . In order to make the remnant polarization disappear, an electric field in the reverse direction has to be applied. At an electric field of $-E_C$ called the coercive field, the polarization becomes zero. If the field is further increased in the reverse direction beyond E_C , the domains get oriented in the direction of the field and the polarization increases with increasing field (in the new reversed direction) until saturation polarization ($-P_S$) is reached in the reverse direction. If the field is now again reduced back to zero, there will be again remnant polarization and increasing the field from zero in the positive direction, the remnant polarization disappears when the field is $+E_C$. Further increase in the field will trace the path to close the loop.

1.3 Electrets

A class of dielectrics that it hasn't been mentioned yet are the electrets, which properties are often related to piezoelectric and pyroelectric materials. An electret is a piece of dielectric material exhibiting a quasi-permanent electrical charge (Figure 1.7). The electret charge may consist of "real" charges, such as surface-charge layers or space charges; it may be a "true" polarization; or it may be a combination of these. While the true polarization is usually a frozen alignment of dipoles, the real charges comprise layers of trapped positive and negative carriers, often positioned at or near the two surfaces of the dielectric, respectively. The electret charges may also consist of carriers displaced within molecular or domain structures throughout the solid, resembling a true dipole polarization. On metallized electrets, a compensation charge may reside on the electrode, unable to cross the energy barrier between metal and dielectric. Mostly, the net charge on an electret is zero or close to zero and its fields are due to charge separation and not caused by a net charge. An electret not covered by metal electrodes produces an external electrostatic field if its polarization and real charges do not compensate each other everywhere in the dielectric. However, as Heaviside already realized in 1892 [21], the fields of an electret may be compensated within a short time period by the relative motion of real charges and dipoles. This is observed in many piezoelectric substances, so usually the definition of electrets includes also some piezoelectric materials [22].

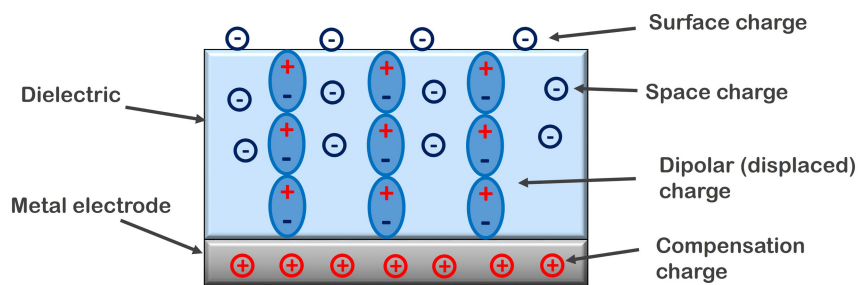


FIGURE 1.7: Schematic cross section of a one-sided metallized electret having deposited surface charges, injected space charges, aligned dipolar charges and compensation charges

1.3.1 Charge formation in electrets

In his early works on electrets, Eguchi [23] found that freshly prepared electrets from wax mixtures, just after removal from the high-voltage electrode assembly, exhibited charges which had sign opposite to that of forming electrodes. That is, the surface which had been in contact with the anode showed a strong negative charge, and the cathode showed positive charge. These initial charges, were found to decay within a few hours or days after the preparation of the electrets. Subsequently they passed through zero and assumed a sign equal to that of the corresponding forming electrode. This type of charge would reach a maximum and then gradually decay with time. This charge was found to be somewhat permanent for all practical purposes, lasting for several years when used for practical applications. Andrew Gemant [24] named the former type of charge “heterocharge” and the latter type of charge “homocharge”. Later, Gross [25] gave the well known “two-charge theory” to explain the behavior of an electret.

Two-Charge Theory

Gross treats electrets from the point of view of absorptive dielectrics. He assumes a decay of electrification caused partly by external and partly by internal conduction within the dielectric itself. The dielectric absorption related to the movement of ions or the orientation of dipoles in the interior of the dielectric gives rise to heterocharge, while the conduction in the dielectric-electrode interface which produces the homocharge. In polar materials, the formation of heterocharge is due mainly to the orientation of the dipoles. With sufficiently high field strengths, conduction currents surge into the interface and consequently electrons are fed into the dielectric or extend from its surface and are transferred to the electrodes. This facilitates the formation of homocharges, which appear in the form of surface charges, later spraying over a certain depth within the dielectric. Because of this process, a weakening of the field occurs which reduces the conduction currents. With short-circuit, a part of the dielectric polarization disappears immediately, and the rest follows more or less slowly. Due to this decay of the heterocharge, the homocharge component begins to prevail in the resulting field. Again, the conduction currents play a role and cause the decay of homocharge, but there is no recombination of these two types of charges [25]. Thus Gross concludes that there exist two types of charges of opposite signs in a short-circuited dielectric. The heterocharge is associated with

dielectric absorption which is due to a homogeneous volume polarization of the dielectric. Homocharge is due mainly to the surface breakdown, which is purely an ionic surface charge. Thus the two-charge theory is capable of explaining the coexistence of the heterocharge and homocharge in a polarized sample and most of the experimentally observed results [26].

1.4 Piezo- and Ferroelectric polymers

By 1927 it was well understood that molecules containing permanent electric moments orient in the direction of an electric field when mobile in the liquid state. Upon solidification of the material in the presence of the field, the dipoles lose their mobility while retaining their preferred orientation. The net dipole orientation produces the electret's permanent polarization (net dipole moment per unit volume). It was also recognized that in addition to the electret's moment there were real charges, generally concentrated near the electret surfaces, which were injected during the formation process by field emission, gas breakdown or similar processes. In 1927 piezoelectricity and pyroelectricity were shown theoretically and experimentally to be properties exhibited by electrets with preferentially ordered dipoles [27]. However, these early wax electrets had poor mechanical strength and low sensitivity, and applications for them did not develop. More recently, strong, highly active polymer films, notably poly(vinylidene fluoride), PVDF, poly(vinyl fluoride), PVF, and poly(vinyl chloride), PVC, have been recognized for their potential value as thermoelectric and electromechanical transducer materials. For this reason a lot of work has been done on production of different kind of synthetic polymers, amorphous and semicrystalline [22]. From the first studies on this class of polymers, was clear that semicrystalline polymers were more promising for potential applications. In particular, in 1969, strong piezoelectricity was observed in PVDF, with the piezoelectric coefficient of poled thin films as large 10 times larger than that observed in any other polymer [28]. Another interesting thing is that at high electric fields, the polarization that occurs in polymers such as PVDF is nonlinear with the applied electric field. This nonlinearity in polarization is defined as hysteresis. The existence of a spontaneous polarization together with polarization reversal is generally accepted as proof of ferroelectricity. Although ferroelectric phenomenon has been well documented in ceramic crystals, the question of whether polymer

crystallites could exhibit dipole switching was debatable for about a decade following the discovery of piezoelectricity in PVDF. Inhomogeneous polarization through the film thickness which yielded higher polarization on the positive electrode side of the polymer led to speculations that PVDF was simply a trapped charge electret. These speculations were dispelled when X-ray studies [29] demonstrated that polarization anisotropy vanishes with high poling field strengths and that true ferroelectric dipole reorientation occurs in PVDF. However, is still a subject of study the role of trapped charges in the polarization stability and orientation. In recent years great improvements have been done on comprehension and realization of this polymer and its related copolymers. These semicrystalline fluoropolymers represent the state of the art in piezoelectric polymers and are currently the only commercially available piezoelectric polymers. In the next sections, it will be given a description of PVDF and its copolymer P(VDF-TrFE) that are the most representative organic ferroelectric polymers and also the subject of this work.

1.4.1 PVDF

PVDF (Poly(vinylidene fluoride)) has a very simple chemical formula, $-\text{CH}_2-\text{CF}_2-$, intermediate between polyethylene (PE) $-\text{CH}_2-\text{CH}_2-$, and polytetrafluoroethylene (PTFE) $-\text{CF}_2-\text{CF}_2-$. The spatially symmetrical disposition of the hydrogen and fluorine atoms along the polymer chain gives rise to unique polarity effects that influence the electromechanical response, solubility, dielectric properties, crystal morphology and yield an unusually high dielectric constant. The dielectric constant of PVDF is about 12, which is four times greater than most polymers, and makes PVDF attractive for integration into devices as the signal to noise ratio is less for higher dielectric materials. The amorphous phase in PVDF has a glass transition that is well below room temperature ($-35\text{ }^\circ\text{C}$), hence the material is quite flexible and readily strained at room temperature. Because of these structural characteristics, PVDF takes many types of molecular and crystal structures, which change depending on the preparation conditions of the samples. The PVDF polymer is typically 50% to 60% crystalline depending on thermal and processing history and has five different phases, called the α , β , γ , δ and ϵ phases [30], among which the α phase is nonpolar and the β phase is the most polar (Figure 1.8). The most stable, non-polar α phase results upon casting PVDF from the melt and

can be transformed into one of the polar phases by mechanically stretching at elevated temperatures or by rotating the molecular chain axis with a high electric field. The β phase is most important for piezoelectric considerations because it has a dipole moment perpendicular to the chain axis.

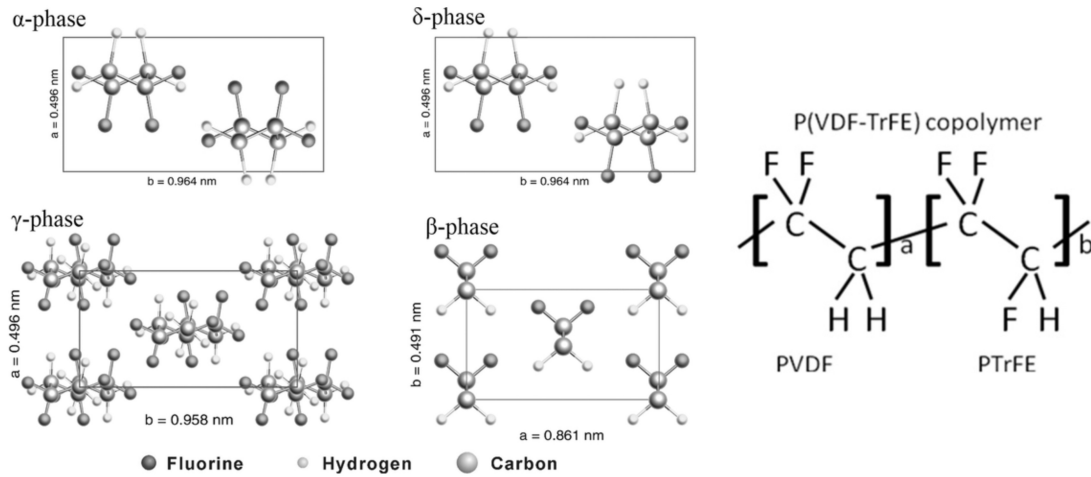


FIGURE 1.8: Representation of PVDF molecules; on the left it is shown the structure of principal crystal phases of PVDF, on the right the changing in structural formula of copolymer PVDF-TrFE [30].

1.4.2 P(VDF-TrFE)

The copolymer P(VDF-TrFE) (poly(vinylidene fluoride-trifluoroethylene)) is of great interest because it crystallizes predominantly in the β phase, readily showing an intrinsic polarization, in fact it has been shown that it exhibits strong piezoelectric, pyroelectric and ferroelectric effects. However, because of the semicrystalline nature of these polymers, PVDF-TrFE can also present a paraelectric phase, even after polymer annealing. The structure of this copolymer, as shown in Figure 1.8, is practically the same as PVDF, with the insertion of PTrFE between consecutive PVDF fundamental units. An attractive morphological feature of the comonomers is that they force the polymer into an all-trans conformation that has a polar crystalline phase, which eliminates the need for mechanical stretching to yield a polar phase. P(VDF-TrFE) crystallizes to a much greater extent than PVDF (up to 90 % crystalline) yielding a higher remnant polarization, lower coercive field and much sharper hysteresis loops. TrFE also extends the use temperature by about

twenty degrees, to close to 100°C [18]. Although the piezoelectric constants for the copolymers are not as large as the homopolymer, the advantages of P(VDF-TrFE) associated with processability, enhanced crystallinity, and higher use temperature make it favorable for applications. The piezoelectric constants d_{33} for highly ordered lamellar P(VDF-TrFE) have recently reached values of about -38 pm/V [31]. Recently, it was shown that geometrical confinement, which leads to a high-aspect-ratio PVDF and P(VDF-TrFE) nanostructures with at least one feature size below 100 nm, could have a profound influence on the final piezoelectric performances of these macromolecules [32]. In particular, preferential crystallization in the polar β phase was shown not only in P(VDF-TrFE) nanostructures but also in PVDF nanowire arrays, and it led to remarkable levels of polarization [33] without further processing the polymer with mechanical stretching or electrical poling, in contrast to the polymer's conventional performance in bulk or thin films. In the next Chapters it will be presented a technique for the production of thin films and nanofibers and a further investigation about the effects of nanoconfinement.

1.5 Applications

In recent years, driven by the rapidly developing miniaturized electronics, new organic devices based on polyvinylidene fluoride (PVDF) and its copolymer with trifluoroethylene (TrFE) have attracted intensive research interest. The great piezo-, pyro- and ferroelectric properties showed by these materials have made them the most promising candidates for a new generation of devices for energy harvesting, nonvolatile memories and sensors. Their attractive advantages include low temperature processing, low-cost solution processing, outstanding chemical stability, and non-toxicity [34]. Previous studies showed how the most effective methods of improving the performance of these materials consist in doping modifications, preparation process optimizations, and dimension lowering strategies. Among this class of materials, low-dimension ferroelectric materials have become widely studied within the field ferroelectric materials research because of the new physical properties and phenomena caused by the reduction of dimensions at nanoscale. The discovery of Langmuir-Blodgett (LB) ferroelectric polymer films in 1995 [35] led to investigation of ferroelectric properties and finite size effect at the nanoscale. Since then, it has been a subject of intensive study not only in theoretical aspects

but also in technical applications. There have been strong debates of the theoretical models used to explain the experiments. Currently, the explanations for the switching behavior in P(VDF-TrFE) thin films are still controversial [36]. Recently, one-dimensional (1D) ferroelectric nanostructures (wires, rods, tubes, belts, and fibers) have been extensively studied because of their specific ferroelectric behaviors related to 1D morphologies. Generally, the specific properties of 1D ferroelectric nanostructures are attributed to the increased surface area. Moreover, decrease in size and dimensionality can facilitate the formation of single domain structures, which can dramatically enhance ferroelectric properties. Therefore, 1D ferroelectric nanostructures present great potential for use in nonvolatile memory devices, microelectromechanical systems, FE-PV devices, nonlinear optics, nanogenerators, and sensors. In recent years, considerable progress has been achieved in the study of 1D nanostructured ferroelectrics (e.g., synthesis, properties, and applications), although barriers to the practical application of nanodevices remain [37]. In this section it follows a brief review of some of the most interesting and cited application based on nanostructured PVDF polymers.

1.5.1 Energy harvesting devices

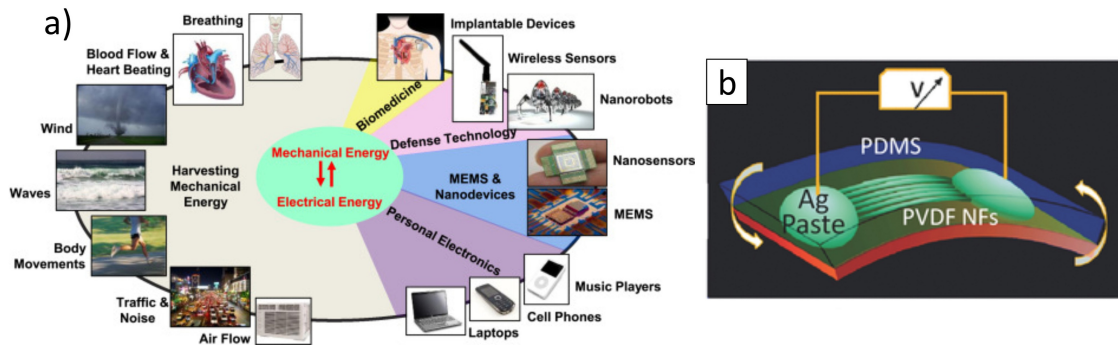


FIGURE 1.9: a) Possible sources of energy for harvesting (left) and opportunities use of this energy in sensing and actuation (right) that can be considered for flexible/bendable piezoelectric devices [38]. b) Example of a P(VDF-TrFE) nanofibers-based device [39].

Energy harvesting is the process by which energy is derived from external sources (e.g. ambient energy), captured, and stored for small, wireless autonomous devices, like those used in wearable electronics and wireless sensor networks. Among these energy sources, mechanical energy may be the most widely distributed and is specialized for human motion-related applications. It exists abundantly as different

forms and is frequently located in our local environment, but the vast majority is ignored and wasted, such as human motion, walking, mechanical triggering, vibration, wind, flowing water and so forth (Figure 1.9a). An outstanding feature of nanogenerators technology is its simplistic and diverse structural properties that can be applied for flexible and stretchable electronics. Flexible electronics are attracting substantial attention because of their promising applications in many areas, such as wearable electronics and bendable displays. The realization of fully flexible electronics demands to have an appropriate flexible power supply device. P(VDF-TrFE) is one of the most interesting materials to create such devices and is commonly used for piezoelectric applications because of his advantageous properties of flexibility, adequate mechanical strength, ease of processing and high chemical resistance. Polymers' chemical stability and biocompatibility is in favor of its application in biological systems, such as implantable sensing and energy harvesting. A notable disadvantage is that achieving good performance requires electrical poling in which mechanical stretching processes need to align the dipoles of the polar β -phase of PVDF structures [40]. During the last decade different kind of devices has been developed by research, most of them were based on thin film structures. Recently it has been demonstrated that better performance can be reached using electrospun P(VDF-TrFE) nanofibers as shown in Figure 1.9b [39].

1.5.2 Nonvolatile Memories

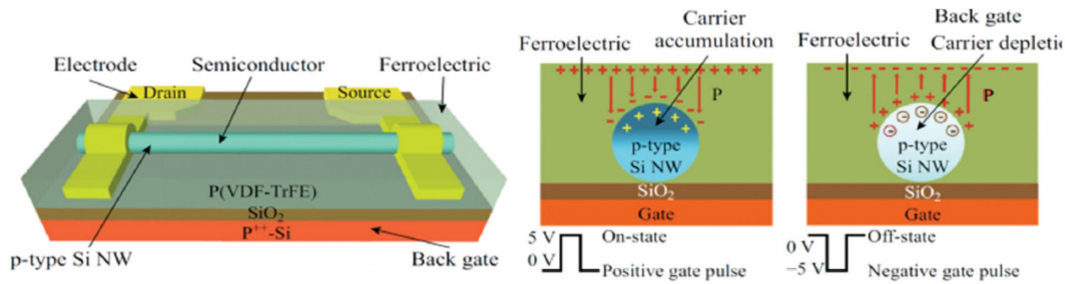


FIGURE 1.10: Schematic view and operating mechanism of a back-gate FeFET-based nonvolatile memory device [41].

Another important application of P(VDF-TrFE) thin films and fibers is ferroelectric nonvolatile memory (Figure 1.10). The principle of nonvolatile ferroelectric random access memories (FRAMs) is based on the polarization reversal by an external applied electric field. The binary logic states “1” and “0” are represented

by the nonvolatile storage of the positive or negative remanent polarization states. The nonvolatile property is due to the fact that the sample can hold the polarization state when the external field is removed. Compared to other nonvolatile memories, for example, flash, electrically erasable and programmable read-only memories (EEPROM) FRAMs have faster write and read times, lower power consumption, and high write and read endurance. FRAMs can be applied in a variety of consumer products, such as smart cards, power meters, printers, videogames, and radio-frequency identification (RFID) tags. The available commercial FRAMs are based on perovskite-type ferroelectrics such as lead zirconium titanate (PZT) but generally require high annealing temperature ($>400\text{ }^{\circ}\text{C}$), which is harmful to other components on the chip. P(VDF-TrFE) copolymer is the promising material to replace perovskites for his already cited properties regarding easy processing, low temperature, low-cost and chemical stability [36]. Although there is advantage in using P(VDF-TrFE) for FRAMs, there are also some practical challenge to overcome in order to commercialize such memory devices. First, an improvement in performance, in fact lots of groups reported a problem of high operational voltage [42]. Second, an appropriate approach must be found to control switching dynamics in the copolymer films. Finally, the solution processing has to be incorporated into the semiconductor-manufacturing process.

1.5.3 Other Applications

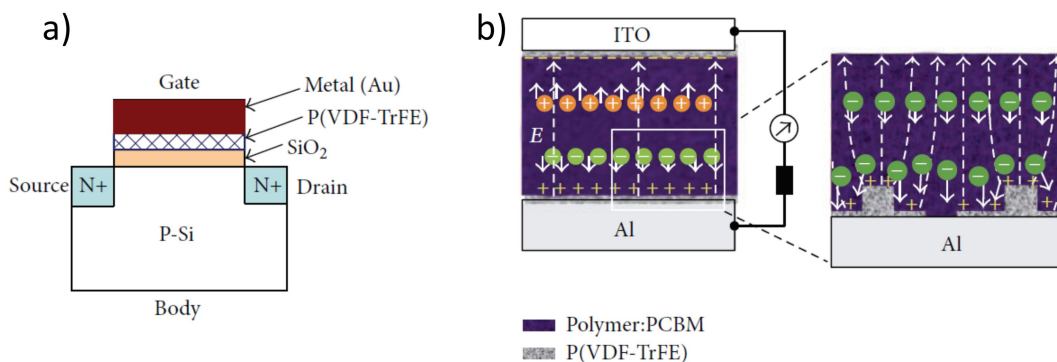


FIGURE 1.11: a) Example of ferroelectric transistor Fe-FET [43], b) structure of polymer photovoltaic devices with FE interfacial layers and a schematic diagram of electric field. The right-hand panel illustrates the electric-field distribution and electron conduction through the P(VDF-TrFE) on the Al side [44].

Negative Capacitance devices

Conventional field-effect transistors (FETs) require a change in the channel potential of at least 60mV at room temperature to induce a change in the current by a factor of 10, which is determined by the Boltzmann limit. Recently the concept of coupling the ferroelectric layer to the channel of a field effect transistor for lowering the subthreshold swing due to the negative capacitance effect is actively studied [36]. This concept is proposed by Salahuddin and Datta in 2008 [45] which opens a new route for the realization of transistors with steeper subthreshold characteristics and thus enabling low power dissipation. The experimental validity of Fe-FET with a sub-60mV/decade switching behavior is firstly demonstrated incorporating a thin P(VDF-TrFE) film into a gate stack. Figure 1.11a shows the device configuration of the negative capacitance FET [43]. The challenges include successful integration of ferroelectric/dielectric gate stacks onto FET structures especially for oxides and efficient designs to ensure hysteresis free operation. More efforts need to be spent to include temperature and interface effects on the device performance.

Photovoltaic devices

Recently it is reported that, by using a permanent electric field of an ultrathin layer of ferroelectric P(VDF-TrFE) introduced at the interface between the electrode and a semiconductor layer in an organic photovoltaic (OPV) device, the charge pair separation and charge extraction efficiency can be increased and thus the power conversion efficiency (PCE) is enhanced by up to 200% [44]. OPV devices have been intensively investigated during the last few years due to their promising application for future low cost and high performance energy sources. The energy loss in OPV devices is mainly caused by the recombination of electrons and holes in semiconducting polymer-fullerene blends. To separate the electrons and holes and prevent their recombination by an external field is essential to increase the OPV efficiency [36]. A large internal electric field can be induced incorporating a ferroelectric layer thus eliminating the need for an external field. The device structure and working principle of the OPV based on a P(VDF-TrFE) thin film are illustrated in Figure 1.11b.

Sensors and actuators

Obviously the electromechanical properties of P(VDF-TrFE) exploited in the production of energy harvesters can be used for the development of highly-sensitive sensors and micro-actuators. Examples of such devices are tactile sensor arrays, inexpensive strain gauges, and lightweight audio transducers. PVDF transducers have the advantage of being dynamically more suitable for modal testing than semiconductor piezoresistive transducers, and more compliant for structural integration than piezoceramic transducers. Another feature of this material is the biocompatibility that allows integration of sensors and actuators with human body in biomedical applications.

Chapter 2

Fabrication Methods

In this Chapter, it is described the fabrication of P(VDF-TrFE) samples, analysed in the course of this work. In each section, the technique of deposition and then the technical details of the samples are illustrated. Two kind of samples was analyzed, a spincoated thin film that it is taken as reference for the piezo- and ferroelectric measurements and different samples with randomly oriented electrospun nanofibers.

2.1 Thin film preparation

The thin film is made of microstructured gratings of an organic ferroelectric polymer and it has been produced at the Max Planck Institute of Mainz from Lenz et al., using a deposition technique called solution micromolding [46]. The procedure is schematically depicted in Figure 2.1a. To allow the fabrication of discrete capacitors, the space between the P(VDF-TrFE) lines has to be backfilled with an electrically insulating polymer. Polymer re-dissolution and stamp swelling have to be avoided, so it has been chosen polyvinyl alcohol (PVA) as the insulating polymer, as its solvent, deionized water, neither swells the PDMS stamp nor dissolves P(VDFTrFE).

The film structure is made of copolymer P(VDF-TrFE) (65-35%) that was purchased from Solvay. The number- and weight-average molecular weight amounted to 147 and 296 kg mol⁻¹, respectively. The average molecular weight of polyvinyl alcohol (PVA) (Sigma-Aldrich) was 80–90 kg mol⁻¹. P(VDF-TrFE) was dissolved in dimethyl sulfoxide (DMSO) and methyl ethyl ketone (MEK). A 400 silicon master with anti-sticking coating provides a periodic line grating with pitch size of 4 mm, line width of 1.3 mm and height of 2 mm. Stamps complementary to the master grating were prepared from poly(dimethylsiloxane) (PDMS) and then is casted

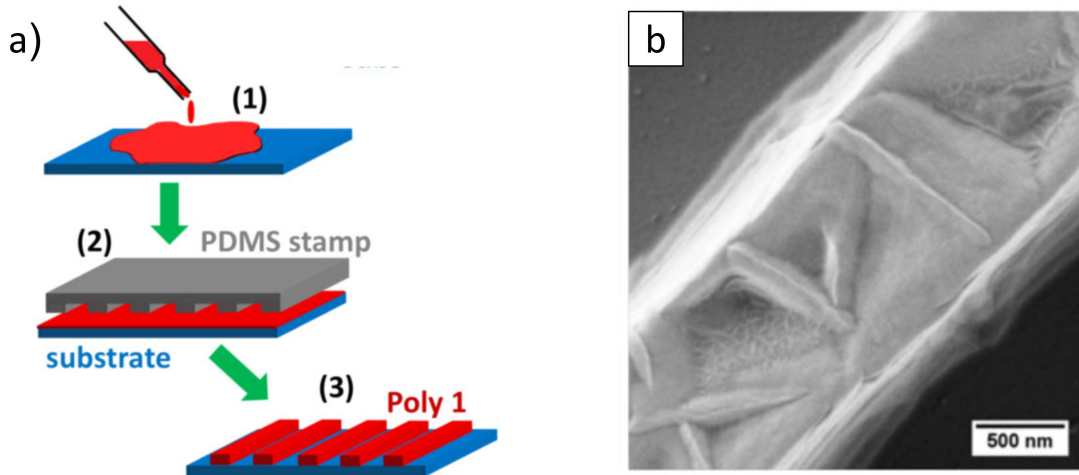


FIGURE 2.1: a) Schematization of solution micromolding procedure and b) SEM micrograph micromolded grating (Figure adapted from [46]).

on the master. The stamp/master assembly was evacuated in a desiccator in order to extract air bubbles. After curing for 3 h at 60° C, the PDMS stamp was peeled off from the master. As shown in Figure 2.1a, polymer gratings were fabricated on glass substrates with bottom electrodes of 100 nm thick Au with a 5 nm Cr adhesion layer, prepared by thermal evaporation through a shadow mask. The substrates were subsequently cleaned with UV/ozone and a drop of the polymer solution, P(VDF-TrFE) in DMSO, was put onto the substrate. The PDMS stamp was positioned on top and the substrate/stamp assembly was hot pressed for 2 h. The temperature for P(VDF-TrFE) was set to 140° C, which is above the Curie temperature (120° C) but below the melting temperature (150° C) of the copolymer. The resulting morphology of the molded gratings is shown in Figure 2.1b (SEM micrograph).

2.2 Electrospun Nanofibers

2.2.1 Electrospinning

Electrospinning process has been known since 1934, thanks to a patent by Formhals consisting in an experimental setup designed for the production of polymer filaments using electrostatic force. Therefore, the term electrospinning refers to a process that produces fibers through an electrically charged jet of polymer solution

or polymer melt. In general, the versatility of electrospinning allows the production of different polymers, blends, fibers containing precursors, suitable for a wide range of applications. A large number of materials can be directly produced by electrospinning, e.g. polymers and polymer composites, while other materials such as ceramics require post processing of the electrospun fibers. Hence, electrospinning is a cheap and simple technique to manufacture nanofibers, thanks to the requirement of common laboratory equipment. However, the science behind this technique is very complex [47].

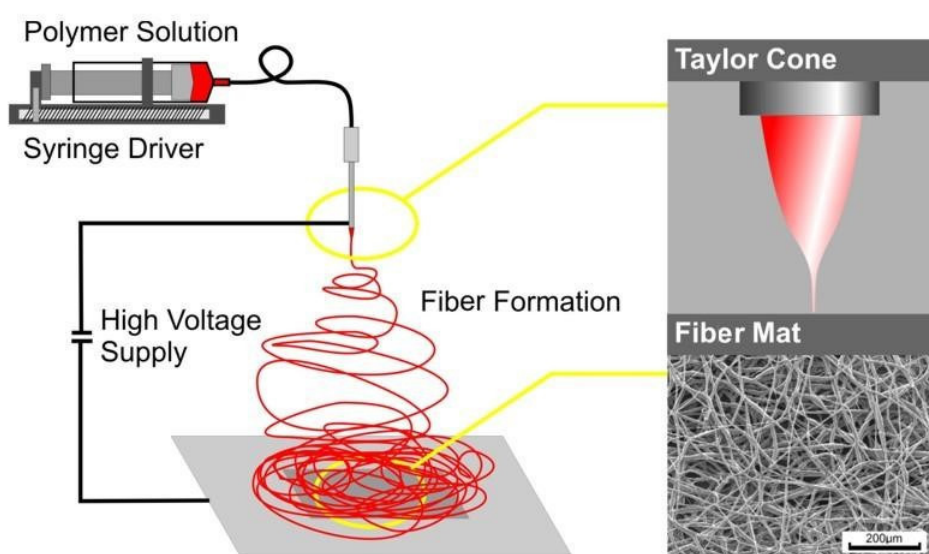


FIGURE 2.2: Sketch of the electrospinning process [48]).

Continuous polymeric or inorganic fibers, can be obtained through electrospinning by a jet of an electrostatically charged molten polymer or a polymeric solution. Typical dimension of electrospun fibers may range from tens of nanometers to a few microns. The charging process take place in an electrified needle through which the polymer solution flows. The needle is connected to a high voltage DC generator (in the kV range) and a collecting grounded electrode, as shown in Figure 2.2. The polymeric solution, electrostatically charged by the high voltage power supply, comes out from the needle tip in the form of a hanging drop. The high electric field between the needle and a grounded electrode causes a distortion of the drop, until it takes a conical shape, called Taylor Cone. For a critical value of electrostatic potential acting on the charged drop, the resultant force exceeds surface tension and a thin jet of fluid polymer is formed and attracted towards the metal collector.

Then, the charged jet is accelerated and stretched by the electric field, undergoing to a process of instability, called whipping instability. The filaments run through a spiral path, which increases the stretching process, thus causing thinning of the fiber while the solvent evaporates. During the path, the whipping instability, allows the formation of fibers with diameters in the order of a few hundred nanometers, favoring the evaporation of the solvent and the solidification of the fibers themselves. The chaotic movement of the jet produces the random deposition of the fibers on the collector. The deposition of aligned fibers is also possible changing the collecting plate with a rotating grounded cylinder, on which the fibers are subjected to an ulterior stretch caused by the rotation [47].

Operational parameters

Some important characteristic parameters of the technique, both related to the polymeric solution and to the electrospinning process, should be pointed out, as they affect the quality of electrospun fibers.

- *Surface Tension*: the charging process of the polymeric solution has to overcome the surface tension, at the same time a too low value of surface tension may cause a jet breakup in to droplets, leading to a process called electro-spraying [49].
- *Polymer Solubility*: conductivity and tendency to be polarized affect fiber morphology during the electrospinning process, high dielectric constant solvents should be used [50, 51].
- *Viscosity*: is directly linked to the grade of bonds formed by polymer chains in the solution, so low viscosity can induce electro-spraying and polymer particles are formed instead of fibers. On the other hand, increasing the viscosity reduces the fiber stretching induced by charges and thicker fibers are deposited. Finally, too high viscosity determines problems to pump the solution through the needle or solution drying creates troubles on the needle tip [50, 52].
- *Polymer molecular weight*: fiber formation occurs only if the molecular weight of the polymer is sufficiently high to give enough viscosity to the solution.
- *Solvent evaporation rate*: evaporation of the solvent, too quick or too slow, during the path towards the collector, can lead respectively to solid fiber

formation or fibers still wet. Environment condition like humidity and temperature affect this parameter.

- *Solution conductivity*: Accumulation of enough charges has to occur in the solution, in order to increase the repulsive forces, thus overcoming the surface tension of the solution. Subsequent stretching of the jet is connected to the ability of the solution to carry charges. The electric conductivity of solvents is commonly very low, due to the presence of very few free ions. A strategy to increase the electrical conductivity of the solution is the addition of a small quantity of a polar non-solvent of the polymer or proper salts. However, the interaction between solvent mixtures can affect polymer solubility, modifying fiber morphology [51].
- *Voltage bias*: provides the stretching of the solution, thanks to the columbic force in the jet and the high electric field. Voltage bias also defines the flight time of the jet, governing the stretching force and consequently fiber diameter. Thinner fiber diameters have been observed increasing voltage bias [50]. Higher voltage bias can also increase the degree of crystallinity of the fibers [53].
- *Flow rate*: this parameter controls how much solution is pushed out from the needle and permits to obtain a stable Taylor Cone, for a given voltage bias. The higher the flow rate, the larger the fiber diameter, due to a bigger volume of solution spun [54].
- *Needle diameter*: the decrease of the inner diameter of the spinneret causes a reduction in fiber diameter; a drop of solution cannot flow through too small needles [55].
- *Needle-to-collector distance*: this parameter is very useful to adjust other already cited feature of electrospinning, because affect electric field strength, flight time and solvent evaporation rate. Too low distance can cause instability in the process [54].

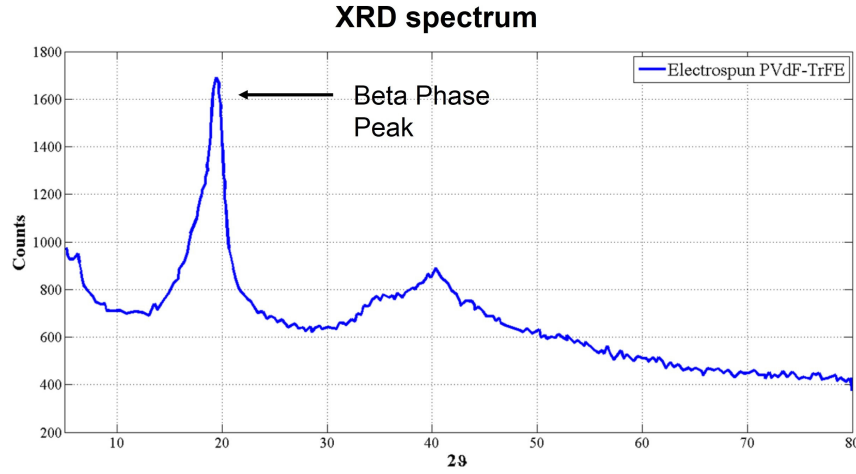


FIGURE 2.3: X-ray diffraction pattern, demonstrating the presence of ferroelectric β phase in the electrospun P(VDF-TrFE) nanofibers[47].

2.2.2 P(VDF-TrFE) nanofibers

The P(VDF-TrFE) nanofibers that will be analysed in this work, were deposited with an electrospinning process. The same copolymer of the thin film, P(VDF-TrFE)(65/35) furnished by Solvay, was dissolved in a solution of acetone (70% vol.) and dimethyl-sulfoxide (DMSO) (30% vol.). The electrospinning process was made with a classical apparatus for the random deposition of fibers at room condition. The regulation of the flow rate was made by the use of a pump that control the flux of solution through the needle, and was set at 1 ml/h. The grounded metal plate was positioned at 15 cm of distance from the needle, that was electrified applying ± 20 kV. Nanofibers were electrospun applying positive and negative bias on Au, ITO and Si/SiO₂ substrates which were connected to the metal collector. The duration of the process was manually limited in order to deposit a thin layer of fibers that allows to perform PFM and KPFM measurements. In Figure 2.3 is shown an X-Ray diffraction spectrum of P(VDF-TrFE) electrospun nanofibers. It can be seen the characteristic peak of the ferroelectric β phase around $2\theta = 20^\circ$. This demonstrate only the presence of the crystal ferroelectric phase, but it is necessary to do further measurements to establish and quantify the real piezo- and ferroelectric properties of this samples.

Chapter 3

Scanning Probe Microscopy techniques

In recent years an increasing number of analytical methods have been introduced for comprehensive analysis at the micron and nanometer dimensions. In particular, great interest has been paid to scanning probe microscopy (SPM), a family of methods allowing visualization of surface structures and examination of their mechanical, electromagnetic, optical, and other properties at such scales. The idea of all SPM techniques is based on the acquisition of information about the interaction that is established between a sharp tip and the surface of samples. In this Chapter I will illustrate the main techniques used for the microscopic analysis of P(VDF-TrFE) samples. The former, called Piezoresponse Force Microscopy, is an advanced technique for the analysis of piezo- and ferroelectric properties at the nanoscale. The latter, is the well known Kelvin Probe Force Microscopy, that has been used for measurements of surface potentials to investigate the electrostatic behaviour of our samples. In order to give a comprehension of these techniques, in general it has been strictly followed the books of Kalinin et al. [56, 57, 58].

3.1 Piezoresponce Force Microscopy (PFM)

Piezoresponse Force Microscopy is a contact SPM mode that is based on monitoring piezoelectric surface displacements induced by the electrically biased probing tip. This method was introduced in 1992 by Guethner and Dransfeld to detect polarized regions in ferroelectric copolymer films and, soon after that, proved to be the most effective approach for the nanoscale study and control of ferroelectric domains in bulk crystals and thin films. PFM is capable of providing a wide range of microscopic information about ferroelectric properties with spatial resolution

of 10 nm such as, static domain configurations, domain switching behavior, slow relaxation processes, and local hysteresis spectroscopy.

3.1.1 Experimental Setup

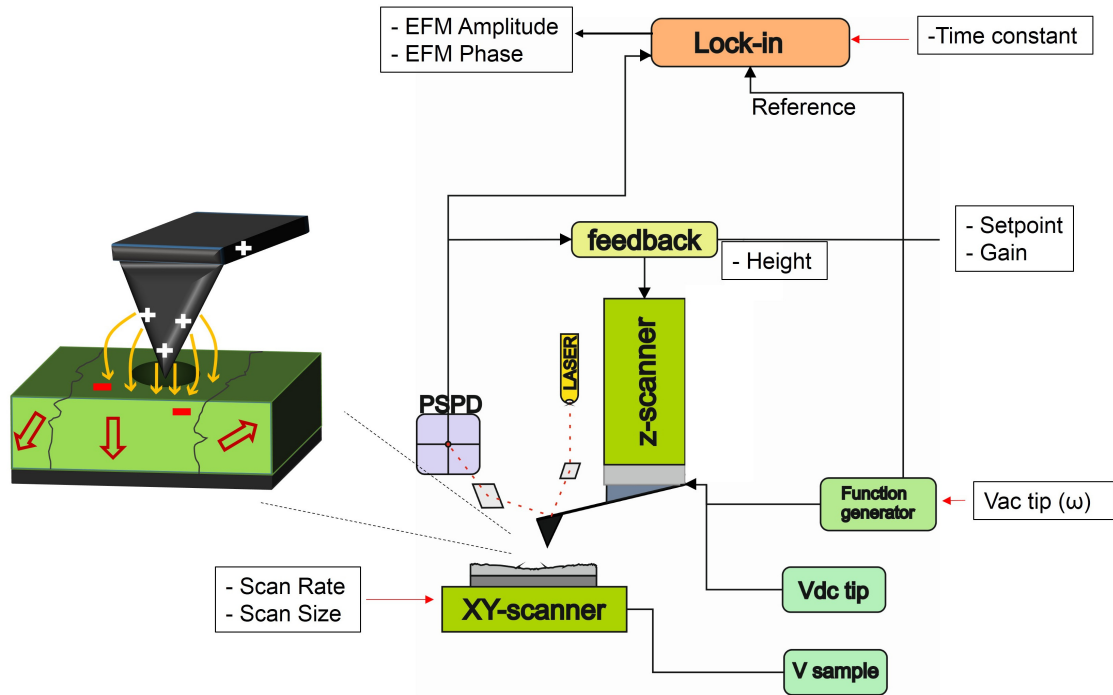


FIGURE 3.1: Typical experimental setup for PFM measurements and details of junction between tip and sample surface, indentation and local electric field.

The standard experimental PFM setup is usually based on a commercial scanning probe microscope as the one illustrated in Figure 3.1. The instrument is equipped with a laser detection based system for the measure of cantilever deflection, a conductive probing tip, a function generator and, at least, one lock-in amplifier¹. For the experiments conducted, it has been used the "Park System NX10" SPM (to have more technical details see [59]). In PFM, a conductive probe makes scans across the surface of a piezo- or ferroelectric sample in contact mode. The conductive cantilever plays the role of the top electrode to provide the localized polarization field to the sample, while the bottom electrode is generally a conductive substrate. The most frequently used probes are either metal-coated silicon probes

¹For the simultaneous acquisition of both vertical and lateral deflection it is necessary to have two lock-in amplifier.

with conducting coatings (Pt/Ir, Au, Rh) or highly doped silicon cantilevers. Measuring the torsion or deflection of cantilever, one can obtain information on the out-of-plane component of electromechanical surface response, i.e., normal to the film plane (vertical PFM, or VPFM), as well as on the in-plane component via the frictional forces (lateral PFM, or LPFM). Application of an AC electric bias to the probing tip results in a sample surface oscillation due to the converse piezoelectric effect. In contact mode operation, the SPM tip touches the sample surface, and the tip-sample repulsive force deflects the tip-cantilever. The cantilever deflection is monitored and used as a feedback signal. Piezoresponse and topography images are acquired simultaneously using the electronic feedback and the lock-in technique. Electronic feedback maintains the “average” force (determined by setpoint) constant and provide to have an accurate tracking of the surface motion, at the same time the lock-in amplifier provides to select the frequency of AC field applied to the tip in order to separate piezoresponse² from height signal. Hence, to prevent attenuation of the out-of-plane piezoelectric response signal, the feedback loop has to operate at a frequency lower than the frequency of the applied voltage V_{AC} . This provides the possibility to separate the PFM signal from the topographical information. Typical operation frequencies for PFM vary from 1–3 kHz to 2–5 MHz, as limited by the bandwidth of optical detector [58].

3.1.2 Elementary theory and applications of PFM

Following the theory already seen, we can resume the relations that describe the ferroelectric materials, in order to understand how PFM works. The strain S_j developed in a piezoelectric material by the applied electric field E_i is described by the matrix equation:

$$S_j = d_{ij}E_i, \quad (3.1)$$

where d_{ij} is the piezoelectric coefficient with the unit of m/V. The indices denote the direction of the electric field and the tensor component of the strain, following the notation used in Chapter 1. Usually, one considers the z axis as the direction normal to the plane of the sample. The main piezoelectric coefficients, are also called longitudinal and transverse piezoelectric constants, respectively if they are measured along the direction of the applied field or in the direction perpendicular to the field. Generally, the longitudinal piezoelectric constant, d_{33} , can be determined

²In practical, the so called piezoresponse is an EFM amplitude signal.

by measuring the displacement (Δz) of the sample along the applied field (E_3):

$$\Delta z = d_{33}V, \quad (3.2)$$

assuming $S_3 = \Delta z/z_0$ and $E_3 = V/z_0$, where V is the applied voltage and z_0 is the thickness of the sample. The measured displacement will be positive, i.e., expansion, if the polarization direction is parallel to the applied field, and it will be negative if the polarization direction is antiparallel to the applied field. In response to the AC voltage $V = V_{AC} \cos(\omega t)$ applied to the tip, the cantilever displacements can be expressed as

$$\Delta z = d_{33}V_{AC} \cos(\omega t + \phi). \quad (3.3)$$

Here, ϕ , represents the difference in phase of the AC voltage applied to the tip and the signal acquired with the PSPD, induced by the deflection of the cantilever.

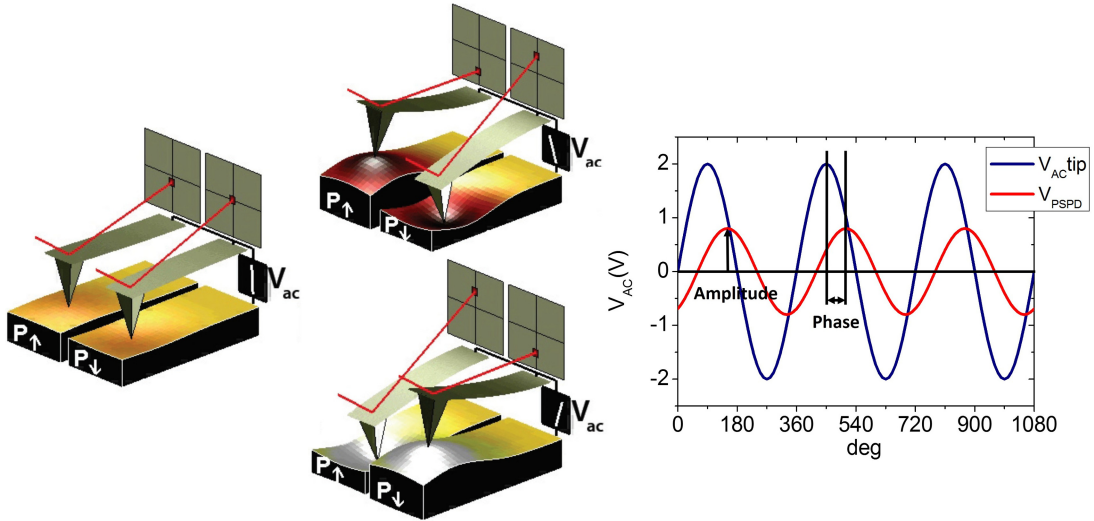


FIGURE 3.2: Schematization of PFM operations and signals. The sample reacts to external AC stimuli inducing deflections of the cantilever that are acquired by the PSPD. Then lock-in amplifier is used to obtain EFM amplitude and phase signal[60].

The phase displacement is due to the coupling between the AC electric field with the internal electric field caused by the orientation of dipoles inside the material (Figure 3.2). Hence, when the polarization points down ($\mathbf{P}_z < 0$) we have $\phi = 0$, while when the polarization points up ($\mathbf{P}_z > 0$), $\phi = \pi$. Therefore, when a small AC modulation being added to the applied electric field, the the cantilever will oscillate in-phase with the AC modulation if the polarization is parallel to the field, and out-phase if antiparallel. Thus, a lock-in amplifier can be used to filter

the piezoresponse signal and to determine both the magnitude of the displacement and the polarization direction of the sample. As already said, the detection of longitudinal piezoresponse is also called vertical piezoresponse force microscopy (VPFM). Because of the presence of non-zero transverse piezoelectric constants, e.g., d_{15} , and the possible misalignment of polarization to the applied field due to a random crystal orientation, an electric field normal to the surface can also cause in-plane shear deformation. This in-plane shear deformation of the sample will give rise to a torsion-like motion to the AFM cantilever, thus results in a change in the lateral signal of a photodetector. Similar to VPFM, another lock-in amplifier can be used to analyse the in-plane piezoresponse signal, obtaining the so called lateral piezoresponse force microscopy (LPFM) measurements.

In addition to imaging, studies of local electromechanical properties can be performed using spectroscopy mode. This kind of measurements is generally performed using a DC bias source, connected in series with the AC voltage source (to the tip or sample), high enough to change the polarization of the material. The hysteresis loops are obtained by sweeping the bias voltage and recording the piezoresponse signal. By analyzing local hysteresis loop measured by PFM spectroscopy, important information about the piezoelectric properties of small ferroelectric domains can be obtained, including coercive voltages, nucleation voltages, forward and reverse saturation and permanent responses. The spatial variations of these parameters reflect the change of local switching behavior of the surface location and nanostructures.

PFM has found major applications in the study of ferroelectric materials (Figure 3.3), particularly for high resolution imaging, domain switching, local hysteresis measurements, and switching of ferroelectric capacitors. For example, one of the first application reliable with local switching of polarization is related to lithographic process. Ferroelectric materials are used in many field effect transistor applications due to their high permittivity. With the increasing demand of miniaturization of electronic devices, it becomes important to study the size effect of ferroelectric materials, i.e., to study the critical size range where significant deviation from bulk properties occurs. The high resolution imaging capability makes PFM suitable for direct measurement of the change of piezoelectric properties with the domain size. Another potential application of ferroelectrics consists in the realization of ultrahigh-density rewritable data storage systems. The high spatial resolution of PFM provides a unique opportunity to study the fundamental process

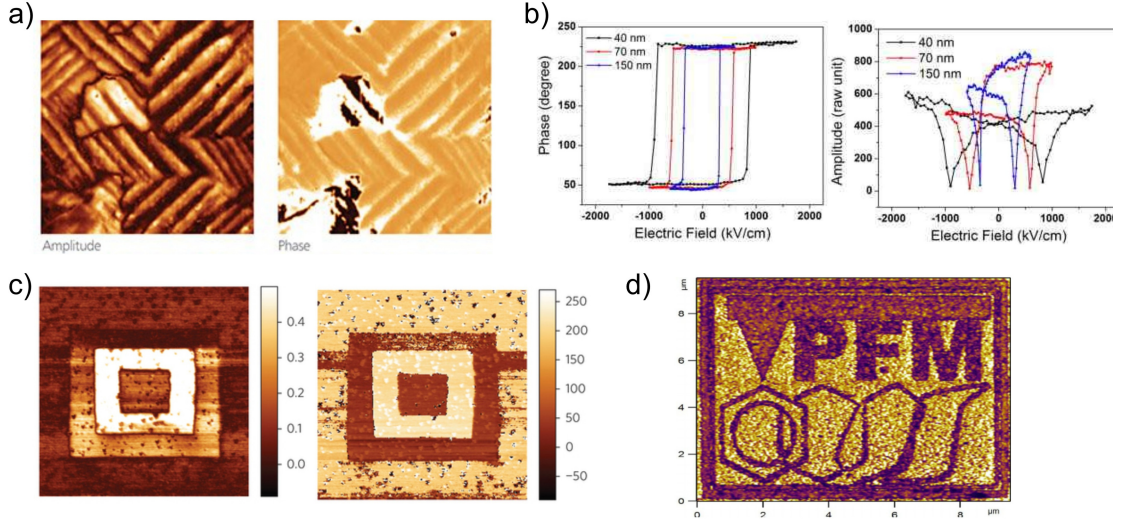


FIGURE 3.3: Examples of results obtained from PFM measurements on ferroelectric materials. a) EFM Amplitude and phase of PZT thin film, showing domains with spontaneous polarization; b) Local hysteresis loops of 40, 70 and 150 nm BFO/LSMO/STO(001) thin films; c) EFM amplitude and phase for a 16-nm-thick BaTiO₃ film poled with +5 V, -5 V and +5 V over 3 μm , 2 μm and 1 μm regions, respectively; d) example of PFM lithography (Figures adapted from [61, 62, 63]).

of domain switching, including the thermodynamics and kinetics of domain nucleation, growth, and relaxation. PFM has also been used to study the switching dynamics of ferroelectric capacitors.

Despite the wide application of PFM in the research of piezoelectric and ferroelectric materials, the imaging mechanism, particular the quantitative interpretation of PFM signals is yet to be fully understood. In the detailed analysis, one finds out that there is an additive contributions of the long-range electrostatic and the electromechanical interactions to the total PFM response:

$$A = A_{el} + A_{piezo} + A_{nl}, \quad (3.4)$$

where A is the total EFM amplitude, and A_{el} , A_{piezo} and A_{nl} are respectively the amplitudes of electrostatic, electromechanical and cantilever-surface capacitive contributions. The presence of A_{nl} results in a constant background to the measured piezoresponse, and it can be minimized by using tall and high aspect-ratio tips. High quality piezoresponse data requires the maximization of the electromechanical contribution and the minimization of electrostatic contribution. The electromechanical contribution depends strongly on the contact interface between the

tip and the surface, the shape, size, and material of the tip itself. The presence of a “dielectric gap” between the tip and the surface below, particularly in the case of “weak indentation” with a soft cantilever, can cause screening of the electric field introduced by the tip, and consequently reducing the piezoresponse amplitude. Therefore, the use of metal coated, stiff cantilever ($k > 1$ N/m) with large force (10-1000 nN, strong indentation) is most desirable for PFM imaging. However, this should be used with caution since, depending on the mechanical characteristics of the investigated material, at high contact forces may occur sample modification and other effects such as stress induced suppression of piezoelectricity. Another concern for quantitative PFM measurement is the calibration of the PFM system [57].

Analysis of First Harmonic Signal

First of all, it is important to establish the origin of the demodulated signals. In other words, one has to know whether and how it is possible to probe the true electromechanical properties of ferroelectric samples. This is because, as mentioned previously, there are two types of forces governing the tip movement above the ferroelectric sample, namely the repulsive contact force and the electrostatic force. Both of these forces act simultaneously on the tip when it is in contact with the sample; therefore the first harmonic of the cantilever deflection is the superposition of their effects. Whether the probe movement is caused predominantly by the electrostatic interaction or by the piezoelectric surface displacements can be determined from the phase value of the first harmonic, as is shown in the following. If an AC voltage $V_{AC} = \sin(\omega t)$ is applied between the conductive tip of the SPM and a bottom electrode located underneath the ferroelectric film being investigated, the film surface oscillates at the same frequency ω , due to the converse piezoelectric effect. Assuming, as before, d_{33} related to the vibration of the surface normal to the film, the movement of the tip when it follows the sample surface displacement is given by the equation 3.3, which here is rewrite as:

$$\Delta z(t) = \begin{cases} \Delta z^+(t) = -d_{33}V_{AC} \sin(\omega t), & P_z > 0 \\ \Delta z^-(t) = -d_{33}V_{AC} \sin(\omega t), & P_z < 0 \end{cases} \quad (3.5)$$

where z is the coordinate normal to the film and P_z is the component of the spontaneous or remnant polarization along the z -axis. If the tip movement is governed by the Maxwell stress force, then the first harmonic of the tip displacement

should be proportional to the first harmonic of this force, F_ω :

$$F_\omega = -\frac{\partial C}{\partial z}(V_{DC} + V_{CPD})V_{AC} \sin(\omega t), \quad (3.6)$$

where V_{CPD} is the contact potential difference, z is the distance between the tip and surface, and C is the tip-to-sample capacitance. To assure proper grounding of all the equipment in the setup, it may be practical to apply the AC voltage to the SPM probe and the DC voltages to the bottom electrode. For a region (ferroelectric domain) with polarization oriented downward (top-to-bottom) and an AC voltage applied to the tip, during the positive half periods (electric field in the film directed downward, i.e. parallel to the polarization), the piezoelectric deformation is an extension, and the surface will move upward. Therefore, the piezoelectric signal is in phase with the applied AC voltage. At the same time, the first harmonic of the Maxwell stress (see F_ω in Equation 3.6, with $\partial C/\partial z$ always positive) and the AC voltage are out of phase. The above considerations lead to the conclusion that if only the electrostatic interaction causes the cantilever deflection, the tip does not follow the vertical displacements of the sample surface, but oscillates out of phase with the induced piezoelectric deformations. Whether the tip vibrates in phase (therefore in permanent contact) with the ferroelectric surface or oscillates out of phase depends on the balance of the contact and electrostatic forces [56].

3.1.3 Calibration of the piezoresponse signal

As already said, the mechanical oscillations of the sample underneath the tip modulate the global deflection signal and are detected using a lock-in technique. Note that it is assumed that the piezoelectric properties are uniform across the films or at least that the d_{33} measured corresponds to an effective value averaged across the film thickness. The piezoelectric constant d_{33} of a given point can be determined as follows:

$$A_{EFM_\omega} = \gamma_{AFM} d_{33} V_{AC_\omega}, \quad (3.7)$$

where A_{EFM_ω} is the amplitude of the piezoresponse signal (PRS), V_{AC_ω} the amplitude of the probing AC voltage and γ_{AFM} is the sensitivity of the system probe-optical detector, which is in fact the conversion factor between the mechanical displacement of the SPM tip and the electric deflection signal. There are two ways to calibrate the PRS. The first one is to use the normal calibration procedure of

the AFM, i.e. a force spectroscopy measurement (used in this work). The second one is to use a standard sample, with a known piezoelectric coefficient, like quartz.

The so-called "detector sensitivity" depends on the following factors: the cantilever through the exact way how it bends under load, the detector itself through how it converts the displacement of the tip into an electrical signal, and finally by the detector electronics which deliver the deflection signal. Therefore, the detector sensitivity is in fact the "instrument sensitivity" and each time the cantilever is changed a new calibration is needed. The calibration of the deflection signal is usually necessary in order to determine the interaction force between the tip and sample, knowing the cantilever spring constant. The procedure for calibration consists in extension and retraction of the cantilever along the z direction while the optical detector acquires the correspondent z -deflection. Initially, the tip approaches the surface in non-contact and the deflection signal is zero. When the tip achieves the contact with the surface, the extension continues pushing the opposite end of the cantilever towards the surface. Thus, the cantilever bends changing the angle of reflection of the laser beam, and therefore the deflection signal. For small bending, the dependence is linear. Since one acquires the variation of electrical signal vs z -scanner displacement, the slope of the linear dependence is the detector sensitivity γ_{AFM} in Equation 3.7.

3.2 Kelvin Probe Force Microscopy (KPFM)

The Kelvin probe force microscopy (KPFM) is a non-contact scanning probe microscopy technique designed to obtain surface potential images with nanometer resolution, by measuring the electrostatic forces between probe and sample surface. Since its first introduction by Nonnenmacher et al. in 1991 [64], KPFM has been used extensively as a unique method to characterize the nano-scale electronic/electrical properties of metal/semiconductor surfaces and semiconductor devices. Recently, KPFM has also been used to study the electrical properties of organic materials/devices and biological materials [65]. Since the KPFM experimental is an Atomic Force Microscopy based apparatus, the basic operational principles and instrumentation of AFM and KPFM are reviewed together

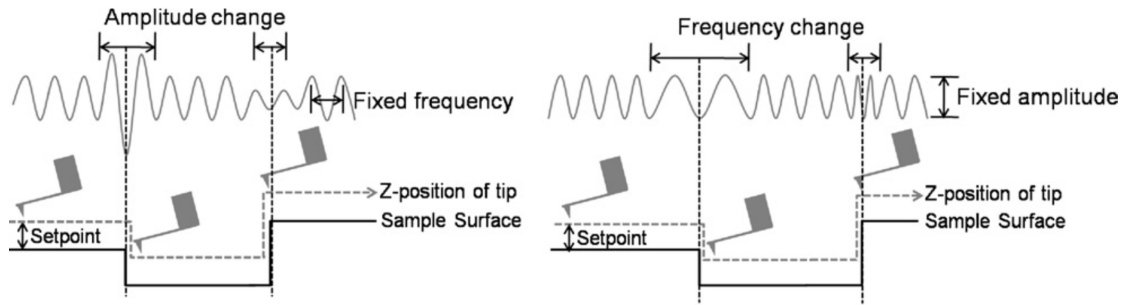


FIGURE 3.4: Schematization of basic non-contact AFM operations. The picture shows both amplitude (left) and frequency (right) modulation mode (Figure adapted from [65]).

3.2.1 Basic principles of non-contact AFM

KPFM is primarily based on the experimental setup of a non-contact AFM system, which provide to the acquisition of high resolution topographic images at the same time of the surface potential images. In non-contact mode, the cantilever is externally oscillated at, or close to, its resonance frequency. The tip-sample interaction is altered as the tip-sample separation changes, because of the structures on the sample surface, leading to a variation of oscillation amplitude and resonance frequency. These amplitude and frequency changes, with respect to the reference amplitude and frequency, are used as feedback signals to obtain the topography of the sample surface. Therefore, non-contact mode is referred as amplitude modulation (AM) and frequency modulation (FM) operation. In the typical range of operation of non-contact AFM, the tip-sample interaction is perturbed by attractive Van der Waals forces, causing amplitude or frequency variations in the oscillation of the AFM cantilever, as illustrated schematically in Figure 3.4. In AM mode AFM, changes in the oscillation amplitude provide the feedback signal for imaging. The amplitude of oscillation increases as the tip-sample distance increases, due to the decrease of tip-sample interaction. The amplitude change is monitored and regulated by a feedback system to keep the tip-sample distance constant at a pre-determined set-point (typically 10-30 nm). The dependence of amplitude variation on the tip-sample interaction can be described analytically, based on the harmonic oscillator model, and the amplitude change is generally considered to be dependent on the force between the tip and sample. Thus, AM mode measurements represent the direct force between the tip and sample [66, 67]. In FM mode AFM, variations in the oscillation frequency provide information about tip-sample interactions. The

cantilever oscillation frequency changes due to the tip–sample distance variation. A feedback system regulates the frequency change to keep the set-point frequency constant, allowing the topography of the sample surface to be acquired. The variations in oscillation frequency are dependent on the force gradient between tip and sample when the restoring force of the cantilever that is associated with tip oscillating energy is large compared to the interaction force between the tip and sample surface [67, 68]. AFM resolution is dependent on the quality factor (Q) of the vibrating cantilever, a measure of the energy loss of the oscillation [66]. Q is defined as the ratio between resonant frequency (f_0) and frequency change (Δf) at full-width-halfmaximum:

$$Q = \frac{f_0}{\Delta f}. \quad (3.8)$$

In air, the typical Q of a cantilever, with typical resonant frequency of 300 kHz, is approximately 100. An expression for the minimum detectable force (δF_{min}) by an AFM is:

$$\delta F_{min} = \sqrt{\frac{2k_l k_b T B}{\omega_0 Q \langle z_{osc}^2 \rangle}}, \quad (3.9)$$

where k_l is the force constant of the cantilever, $k_B T$ is the thermal energy at the ambient temperature, B is the measurement bandwidth, ω_0 is the resonant frequency of tip, and $\langle z_{osc}^2 \rangle$ is the mean-square amplitude of the driven cantilever vibration [68].

In an AFM system, the acquisition of signals is typically provided from tip–sample interaction monitoring (laser and position sensitive detectors) and feedback system. The tip oscillation is detected through the laser beam movement by a position sensitive photo detector (PSPD). A Lock-in Amplifier is used to select (in frequency) and amplify the PSPD signal. The amplitude signal of the tip oscillation feeds into the amplitude feedback system, which controls the z -position of the tip to maintain a constant tip–sample interaction [65].

3.2.2 Fundamentals of KPFM

The KPFM measures the contact potential difference (CPD) between a conducting AFM tip and a sample, which is defined as follow:

$$V_{CPD} = \frac{\Phi_{sample} - \Phi_{tip}}{q} = \frac{\Delta\Phi}{q}, \quad (3.10)$$

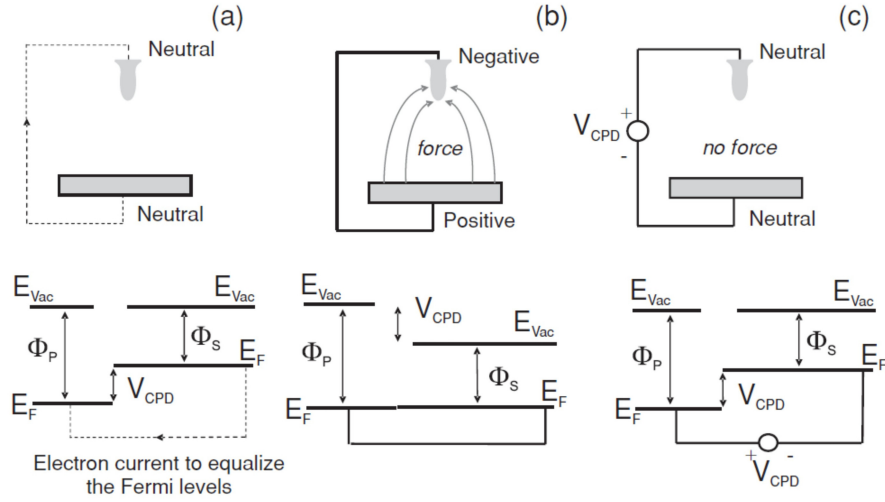


FIGURE 3.5: Schematization of energy levels of sample and SPM tip, related to the correspondent experimental situation. a) Tip and sample are separated by distance d with no electrical contact, b) tip and sample are in electrical contact, and c) external bias (V_{DC}) is applied between tip and sample to nullify the CPD (Figure adapted from [57]).

where Φ_{sample} and Φ_{tip} are the work functions of the sample and tip, and q is the elementary charge. Therefore, if an AFM tip and a sample with different work functions are held in close proximity, an electrostatic force will developed between them, due to the potential difference V_{CPD} ; this is schematically described in Figure 3.5. When the two materials are not connected their local vacuum levels are aligned but there is a difference in their Fermi levels. Upon electrical connection, to reach equilibrium the Fermi levels will align through electron current flow, as shown in Figure 3.5a. The alignment of Fermi levels leads to a displacement of vacuum levels and the charging of both tip and sample surfaces. Hence, as shown in Figure 3.5, an electrostatic force due to V_{CPD} develops between the two electrodes. This force can be nullified by applying an external bias (V_{DC}), between the tip and the sample. The magnitude of this bias represents the contact potential difference and its sign depends whether it is applied to the sample or to the tip (Figure 3.5c). A typical KPFM measurements is conducted by applying an AC voltage (V_{AC}) at frequency ω (typically 10-30 kHz), different from the resonance frequency of the tip, to induce an electrostatic force component at this frequency. To measure the electrostatic force F_{es} separately from other forces (mainly Van der Waals and chemical forces), V_{AC} at frequency ω is superimposed on the tip-sample voltage

V_{DC} . The total applied voltage:

$$V = (V_{DC} - V_{CPD}) + V_{AC} \sin(\omega t), \quad (3.11)$$

results in an oscillating electrostatic force, inducing an additional oscillation of the cantilever at frequency ω . The force which is the derivative of the electrostatic energy with respect to the tip-sample separation, z , is given by:

$$F_{es} = -\frac{1}{2} \frac{\partial C}{\partial z} [(V_{DC} - V_{CPD}) + V_{AC} \sin(\omega t)]^2, \quad (3.12)$$

where $\partial C/\partial z$ is the gradient of the capacitance. This expression can be rewrite dividing the electrostatic force in his different contribution:

$$F_{es} = F_{DC} + F_{\omega} + F_{2\omega}, \quad (3.13)$$

with the components

$$F_{DC} = -\frac{\partial C}{\partial z} \left(\frac{1}{2} (V_{DC} - V_{CPD})^2 + \frac{1}{4} V_{AC}^2 \right), \quad (3.14)$$

$$F_{\omega} = -\frac{\partial C}{\partial z} (V_{DC} - V_{CPD}) V_{AC} \sin(\omega t), \quad (3.15)$$

$$F_{2\omega} = +\frac{\partial C}{\partial z} \frac{1}{4} V_{AC}^2 \cos(2\omega t). \quad (3.16)$$

The DC component F_{DC} results in a static deflection of the AFM tip and contributes to the topographical signal, the term F_{ω} at the frequency ω is used to measure the CPD, and the contribution $F_{2\omega}$ can be used for capacitance microscopy [57]. The simplest approximation of this modelization is to treat the tip-sample system as a parallel plate capacitor with one plate being the tip apex, and the other the sample underneath it.

The force component at frequency ω is proportional to the CPD and therefore can be nullified using a feedback loop. KPFM measures topography concurrently with V_{CPD} . Thus, a method to separate the topographical signal from the V_{CPD} measurement is required. In the KPFM experimental setup (Figure 3.6), the V_{AC} is usually modulated at a frequency higher than the bandwidth of the topography feedback system to prevent cross-talk between topography and CPD measurement. As we can see in Figure 3.6, a V_{DC} , V_{AC} and a second lock-in amplifier is added to the described non-contact AFM system, in order to acquire simultaneously the

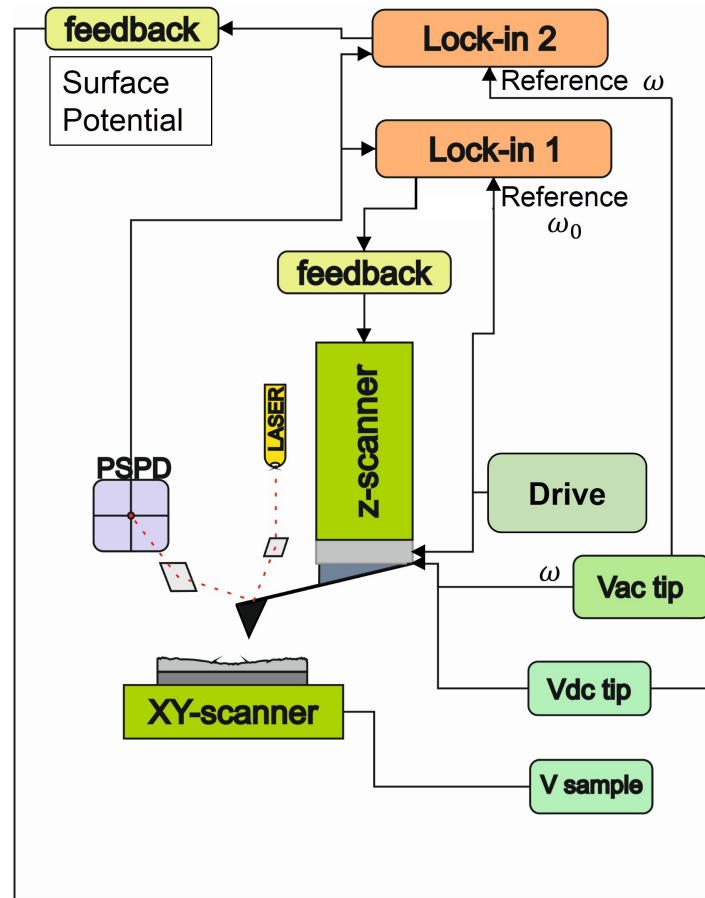


FIGURE 3.6: Scheme of typical apparatus for KPFM measurements. One can notice the structure described for the non-contact AFM mode and the second lock-in amplifier needed for the acquisition of signal at frequency ω .

topography and contact potential difference signals. The second lock-in amplifier (Lock-in 2), is employed to extract the electrical force component with frequency ω (F_ω), so to measure the V_{CPD} . The output signal of the lock-in amplifier is directly proportional to the difference between V_{CPD} and V_{DC} . The V_{CPD} value can be measured by applying $V_{DC} = V_{CPD}$ to the AFM tip, such that the output signal of the lock-in amplifier is nullified and F_ω equals zero. Subsequently, the value of V_{DC} is acquired for each point on the sample surface, composing a map of the work function or surface potential of the hole sample surface area [65].

Chapter 4

Results and Discussions

In this chapter, I will present the most important results from the experiments made on P(VDF-TrFE) thin films and electrospun nanofibers. An explanation and interpretation of the data will also be proposed. The chapter starts with a description of the experimental setup developed during this thesis to characterize piezoelectric hysteresis loops by AFM. Then the data obtained on P(VDF-TrFE) thin film and nanofibers will be presented and analyzed. In the last part I will discuss the relationship between the electrostatic and piezoelectric properties displayed in the examined samples.

4.1 Implementation of SS-PFM

As already pointed out in the previous chapter, a challenge in acquiring the characteristic piezoelectric hysteresis loop by AFM is the superposition of different interactions between probe and sample. In order to obtain hysteresis loops, a variable voltage has to be applied between tip and sample, in a range wide enough to produce an electric field capable to change the polarization state in both directions. The application of such electric field, induces an electrostatic attraction between the conductive probe and substrate. Hence, when the probe is in contact with soft ferroelectric polymers, like the P(VDF-TrFE), the presence of external fields induces the tip to penetrate the material, resulting in a deflection of the cantilever that is measured by the PSPD. To avoid superposition of electrostatic and piezoelectric deflections during the application of high electric fields, which render the acquisition of pure piezoelectric hysteresis loops impossible, the so-called Switching Spectroscopy Piezoresponce Force Microscopy (SS-PFM), has been suggested in previous works.

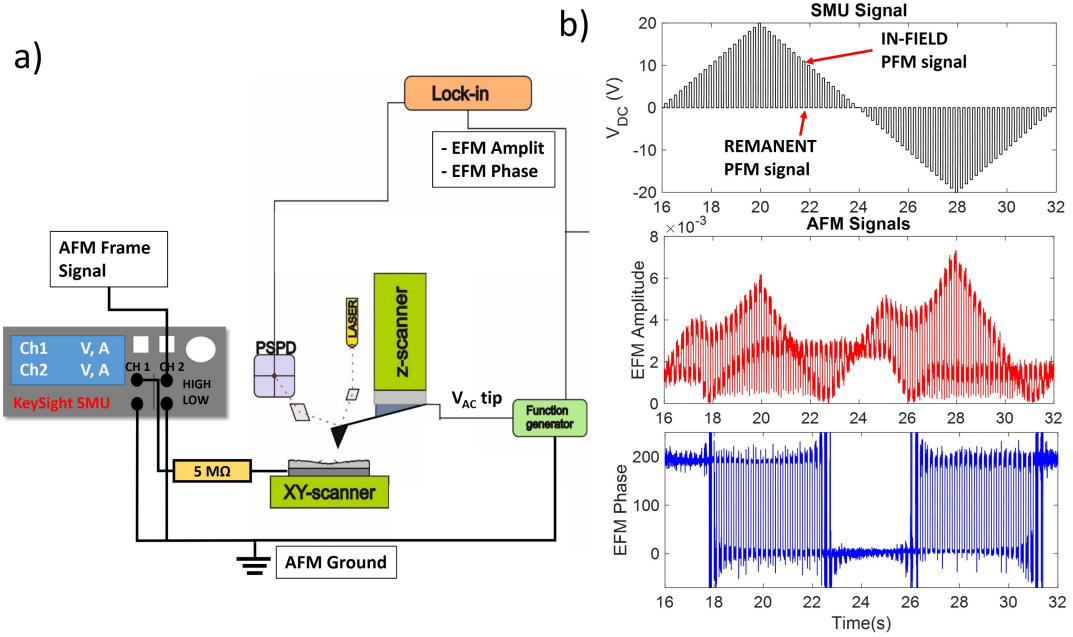


FIGURE 4.1: a) Experimental setup for SS-PFM measurements and example of generated function, b) comparison of typical time-traces used to generate hysteresis loops.

The basic idea behind this technique consists in the application of a variable voltage pulses and in the acquisition of PFM signals during the OFF state voltage, between two consecutive high pulses. Thus, one collects the remnant polarization left from each step right after the application of the field, eliminating the possibility to acquire also a signal component due to the electrostatic interaction. The setup realized for the implementation of this technique is shown in Figure 4.1a. A two channel Source Measure Unit (Keysight b2900a) has been connected to the microscope (Park NX10 AFM). One channel of the SMU provided rectangular voltage pulses (also high voltage)¹ to the conductive sample holder. The second channel was used to acquire the frame signal from the microscope, necessary to achieve synchronization between the acquired AFM-channels and the applied voltage pulses. All signals had a common reference that is the AFM ground. The frame signal gives information about the time interval of scan, so it is necessary to synchronize data collected from SMU and information extracted from the image acquired by the microscope. In Figure 4.1b are shown the traces acquired separately by SMU and AFM against time. The V_{DC} and frame signal time-traces were acquired from

¹For precaution it was inserted a resistance of about 5 MΩ to limit the maximum current that could flow through the setup.

SMU, while EFM amplitude and phase traces were extracted from AFM images with 0 scansize. Then, combining the data, plots of PFM signals against sample bias were constructed, taking the AFM frame signal as reference.

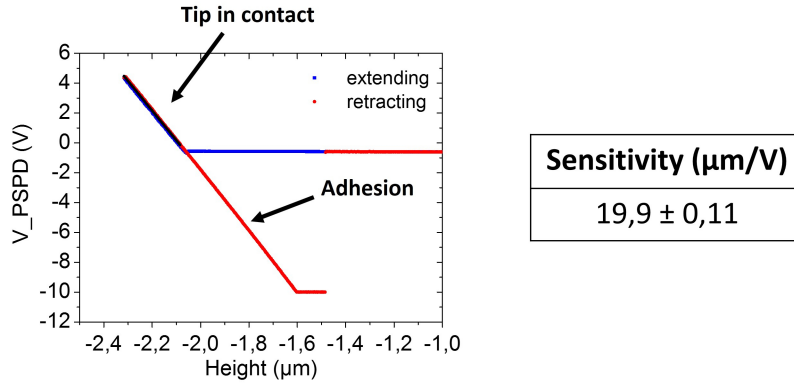


FIGURE 4.2: Force spectroscopy measurements and the resulting value of probe's sensitivity.

In order to analyze quantitatively the AFM data, the sensitivity ($\mu\text{m}/\text{V}$) of the probe used in the PFM experiment has to be measured². All piezoresponce signals are acquired in units of voltage as they always refer to deflections of the cantilever measured with the photodiode. The sensitivity is the parameter for the conversion of voltage in unit of length describing quantitatively the cantilever deflection. Figure 4.2 shows the results of force spectroscopy measurements in which the Z-scanner is forced to move up and down for a definite range of distance also after the tip establishes contact with a rigid surface (here gold on glass). The plot shows curves of extension and retraction from the sample surface. As explained in Chapter 3, it can be noticed that the probe deflects linearly after contact, so fitting that portion of the plot one obtain the relationship between the movement in z-axis and the deflection acquired by the position sensitive photo detector (PSPD). The behaviour shown in the return curve is due to adhesion of the tip which delays the separation from the sample surface, resulting in a deflection of the probe in the opposite direction. From these measurements a sensitivity of $(19.9 \pm 0.11) \mu\text{m}/\text{V}$ is obtained and it was used to do conversions from voltage to picometer.

²In these PFM measurements it was used a diamond coated CDT-CONTR probe with a force constants of 0.5 N/m, applying forces of 4-10 nN.

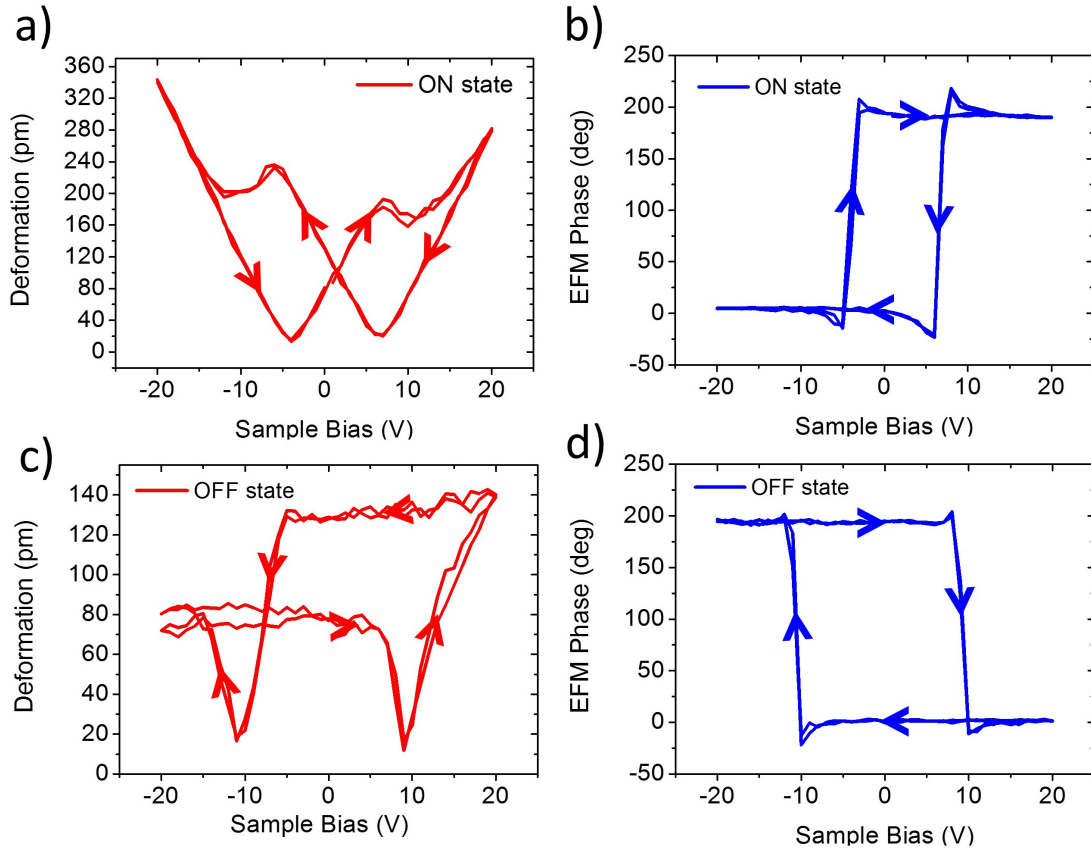


FIGURE 4.3: Comparison of SS-PFM results demonstrating a decoupling of electrostatic and piezoelectric interactions. ON and OFF state data came from the same measure and the AC voltage applied to the tip was $V_{AC} = 3$ V; a-b) typical hysteresis and butterfly loops of piezoresponse and polarization during application of voltage; c-d) hysteresis loops during OFF-state of the applied step function.

Figure 4.3 shows an example of hysteresis loops acquired with SS-PFM on a ferroelectric thin film reference sample, related to both ON and OFF external potential. All plots was obtained from a single scan, separating the data related to time intervals in which the potential was high with the ones related to time intervals in which the potential was zero. It is clear that electrostatic interaction give a massive contribution to the signals when there's an applied voltage. Considering the plot regarding the deformation of the sample, one can notice that in the OFF state the plot represents the typical trend expected for piezoelectric materials, while in the ON state there's a linear dependence of the deformation with the applied field. In the case of ON state, the trend is due to both electrostatic attraction between tip and the grounded conductive substrate, and the deformation of the

sample. The electrostatic attraction increases linearly with the external DC electric field, covering the signal induced by the deformation (for higher DC field the piezoresponse becomes negligible). In the case of OFF state, the trend is strictly dependent on the polarization since the absence of high DC field, in fact there is a maximum of piezoelectric response when the sample is in saturation states and a minimum when the polarization is zero. Moreover, it is interesting to look at the polarization hysteresis loops, that show a radical difference in the orientation of the cycle. This is caused by the difference of the forces combination between tip and sample in the two situations. When the external pulsed voltage is in the high state, the electrostatic interaction dominates and we see the trend relative to the condition of electrostatic repulsion or attraction³. On the other hand when there's no voltage applied, the variation in phase depend to extension or compression of the sample in relationship to the orientation of polarization and the V_{AC} applied on the tip. In the normal piezoelectric effect one has an extension when the AC field is in the same direction of the polarization and a contraction when the orientations are opposite. Analyzing the hysteresis loop in the OFF state in relationship with the polarization induced by the ON state and the oscillating AC field, one realizes that the phase is shifted of 180° compared to the characteristic behaviour of piezoelectric effect. For example, when negative DC bias is applied to the sample, the polarization left in the OFF state is downward and the deformation induced by the AC field should be an extension when V_{AC} is positive and viceversa. Thus, deformation and V_{AC} should be in phase when V_{DC} is negative, and out of phase when V_{DC} is positive. In the hysteresis loop one observes the opposite, hence the sample presents negative piezoelectric effect and d_{33} is actually, a negative value. As will be discussed in the next section, a negative d_{33} value is justified for the material P(VDF-TrFE). For this reasons, it will be always shown only the OFF state plots, since they are the ones which gives the reliable information about piezoelectricity.

4.2 PFM on P(VDF-TrFE) thin film

The first batch of data presented regards a series of experiments made on a P(VDF-TrFE) thin film sample. This sample was used also as reference for the optimization of PFM and Switching Spectroscopy PFM techniques.

³DC voltage was always applied to the sample, so the phase plots may appear reversed.

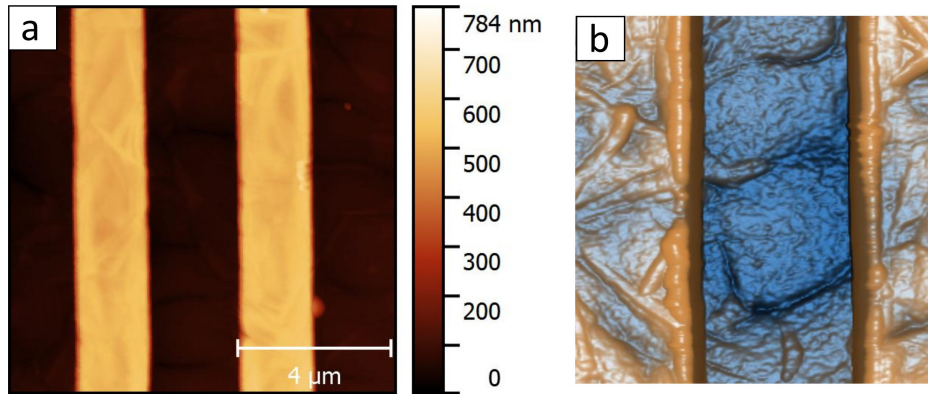


FIGURE 4.4: a) Contact AFM morphology image of the PVDF-TrFE thin film grated sample surface, b) gradient image to underline structural details.

Figure 4.4a shows that, the film structure consists of wells and grooves with a spacing of about 2 microns. The thinner parts of the sample have a thickness of about 100 nm, while the grooves reach 650-700 nm. The separation between consecutive structures is large enough to allow an independent investigation of properties related to both film thicknesses. Figure 4.4b represents a gradient topography image showing a zoom of the sample surface with a well in the center. The high contrast of this image clarifies the fine structure of the P(VDF-TrFE) film, displaying some crystalline structures together with amorphous phase all over the sample. The crystallites seems to be randomly oriented and they have a long and thin shape with variable dimensions around tens of nanometers thick and hundreds of nanometers long. I executed lots of PFM scans and spectroscopies in different position of the sample obtaining results that are useful to make later comparisons with the experiments on nanofibers of the same material.

In Figure 4.5a-b) one can observe the plots obtained by SS-PFM on one well of the sample in an area that was initially polarized with a positive voltage. The applied rectangular voltage pulses start from 0 V reach +20 V and then -20 V to end again at 0 V, the time step is of 100 ms with a duty cycle of 1. This cycle was repeated for at least 2 times in each SS-PFM acquisition. Both graphs display the predicted and characteristic trend of strain and polarization. Looking at the polarization hysteresis loop it can be estimated a coercive potential of about 20 V, necessary to switch from one state of polarization to the other. It also can be noticed that the cycle is squared and symmetric with respect to 0 V. Piezoelectric oscillation amplitude versus sample bias instead, gives us information about the

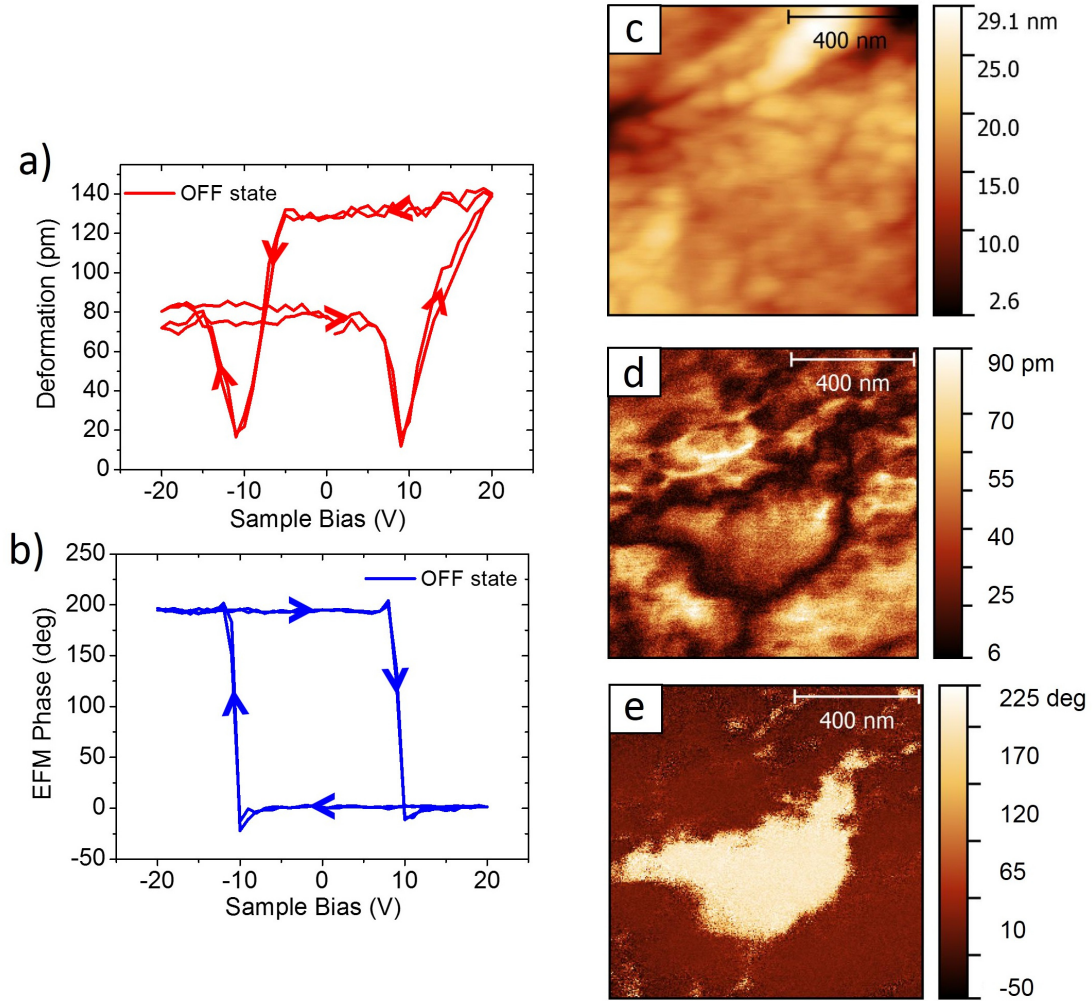


FIGURE 4.5: PFM on 100 nm thick $P(\text{VDF-TrFE})$ thin film; a-b) remnant EFM amplitude and EFM phase signals obtained during cycling voltage from -20 to 20 volts, c-d-e) 1 micron images of height, EFM amplitude and EFM phase acquired after the poling process induced by SS-PFM measurements.

piezoelectric response of the film well, that can be estimate of about 100 pm. In this case there's a certain asymmetry of the trace, correspondly to 0° of phase it can be observed higher values of piezoresponse compared to the one with phase at 180° . An explanation of this phenomenon could be related to electrostriction, that is polarization independent, i.e. it depends only from the electric applied field. Thus, since V_{AC} provide to enhance and decrease the DC field, electrostriction could cause constructive and destructive interferences in EFM signals respectively when the AC field is in phase or out of phase. Another possibility is that the dipoles are aligned and pinned at one of the interfaces.

Doing SS-PFM measurements, implies the application of external voltage high enough to reach saturation polarization, thus a reorientation of ferroelectric domains under the tip, in the same direction of the last applied electric field. Figure 4.5c-d-e) shows respectively morphology, EFM amplitude and phase signal acquired with no DC potential applied after a hysteresis loop characterization. Piezoresponce image displays clearly the formation of one domain delimited by domain walls, which extend around the previous position of the tip. Phase image represents the remnant polarization left after the SS-PFM cycle consistent with the value suggested by the hysteresis loop and with the same shape of the domain already cited. This domain is surrounded by an area with opposite polarization direction that was left from the initial larger scan with positive applied potential.

The next step is to verify the reproducibility of the measurements also with an increased thickness of the film. Then, I repeated the same experiment described above, on grooves, increasing the value of DC potential until I got the results presented in Figure 4.6. As expected, the first thing that one notices is the significant rise of coercive potential which reaches a value of about 80 V (Figure 4.6b). To understand that, one could think to the system made of probe, film and substrate as a capacitor. The electric field, in first approximation, is given by V/d , so being the ferroelectric coercive field a characteristic of the material, increasing thickness made necessary higher voltage to reach the saturation condition. The induced deformation is instead barely the same with respect to the one on the well (Figure 4.6a), in this case the reason is related to the d_{33} constant that is independent from the thickness of the sample. In both plots one can notice less stability of the traces which do not follow the same path during consecutive cycles and a decentralization from 0 V of the polarization hysteresis loop, maybe for the presence of stronger and less stable interactions during the spectroscopy. Again it can be noticed a higher level of piezoresponce corresponding to EFM phase at 0° . The application of high potentials had an evident impact on the surface of the film, in fact in Figure 4.6c we can see the hole left by the tip which had penetrate the sample because of the strong electrostatic interaction. Analysing the image and extracting the profile, I estimated a diameter of the hole of 230 nm at the surface and a depth of 80 nm. In Figure 4.6d-e) it can be seen a behaviour similar to the one observed on the well, the polarization out of plane extends from the center without particular preferential direction. Applying a stronger potential means also to spread the electric field from the tip, for that reason one of the difference that

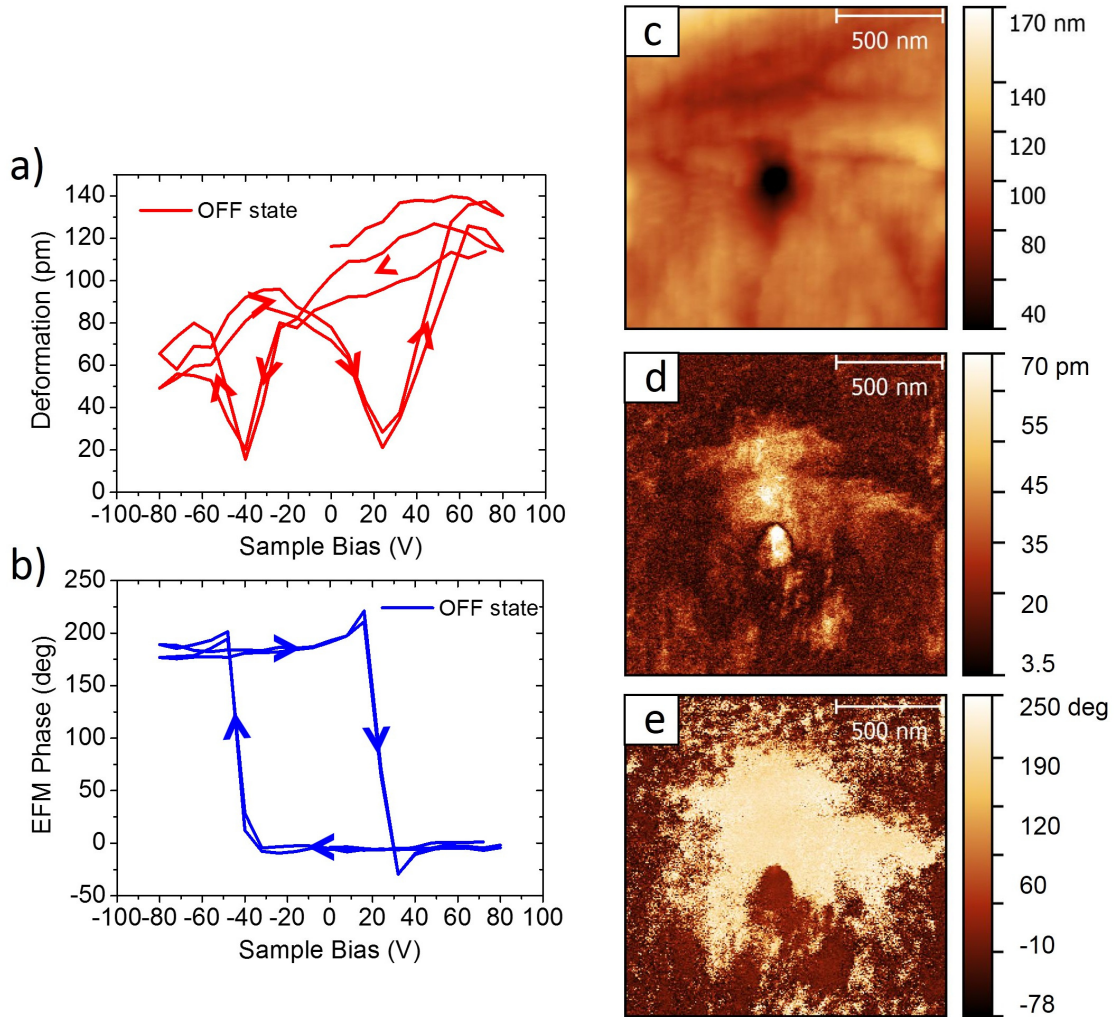


FIGURE 4.6: PFM on 650 nm thick $P(\text{VDF-TrFE})$ thin film; a-b) remnant EFM amplitude and EFM phase signals obtained during cycling voltage from -80 to 80 volts. c-d-e) 1.5 micron images of height, EFM amplitude and phase acquired after polarization process caused by SS-PFM.

we can notice from the well images is a larger extension of the poled area. Another interesting feature of the images taken after the application of high potential, is the presence of small spots with strong signals, corresponding to the position of the tip during SS-PFM. An explanation for this behaviour is related to a possible ionization process induced nearby the tip when the applied potential is higher than a certain level, i.e. the extraction of charge from the material right under the tip which can lead to recurrence of strong electrostatic interactions that have an opposite phase signal compared to the piezoelectric one. This process may represent one

more possible justification for the asymmetry showed by the piezoresponse loop. In this case it was not done an initial scan with opposite applied potential, so the external zones in the images have random polarization (Figure 4.6e) and a low piezoresponse signal (Figure 4.6d), so it is also more difficult to recognize domain walls because of the absence of net borders.

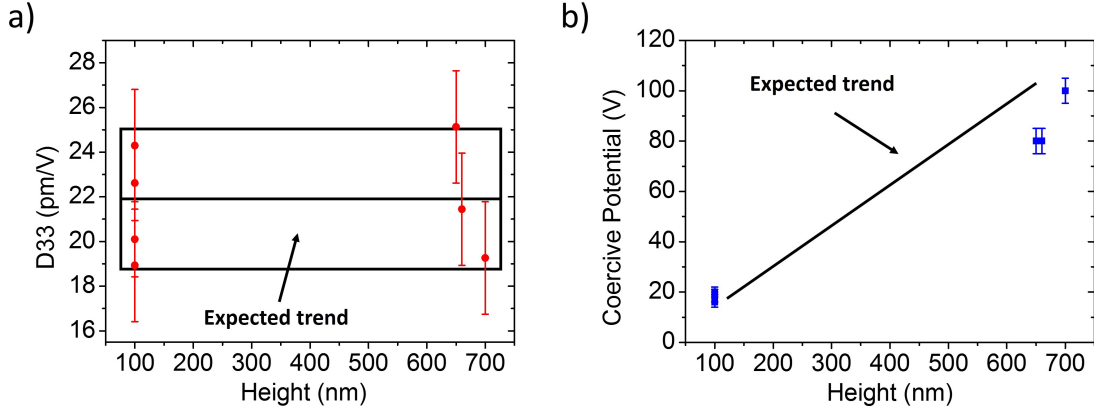


FIGURE 4.7: Relationship between thickness and a) d_{33} , b) coercive potential. The black lines represent the theoretical dependence that one should observe for these parameters, in the d_{33} plot was used the mean value with his uncertainty.

In order to observe the behaviour already discussed of d_{33} and the coercive potential related to the height of the film, repeated measurements were performed on different position over the sample. Because of the morphology of the film, there's practically only two different thicknesses to analyse, so only few values of d_{33} are reported to give a qualitative representation of the expected trend of this parameter. To obtain values for the piezoelectric strain constant I used the relation:

$$d_{33} = \frac{EFMAmplitude(V)}{Sensitivity(V/\mu m) \cdot V_{AC}(V)}, \quad (4.1)$$

where V_{AC} is the 17 kHz alternate potential applied to the tip, usually set at 3 V. As we can see in Figure 4.7a, the values presents quite big uncertainties, but calculating the mean value, one obtains $d_{33} = (21 \pm 3)$ pm/V for 100 nm and $d_{33} = (22 \pm 3)$ pm/V for 650-700 nm of thickness, showing that there is not dependence from height. In Figure 4.7b is shown the difference of coercive potential measured in some wells and grooves. Having only two different thicknesses to measure on,

the number of points is not enough to be sure that there is a linear dependence between height and coercive potential but they give an idea of the necessary increase of voltage to switch polarization when the thickness of thin film changes. All of these results have a good grade of reproducibility. In literature, one can find different values of d_{33} for P(VDF-TrFE) thin films, reaching values of -38 pm/V from macroscopic measurements[31]. This value of d_{33} is greater than what I registered in the film, even if the order of magnitude corresponds. Furthermore, molecular modelling predicted the negative value of d_{33} [69], and also X-ray measurements [70] demonstrated that P(VDF-TrFE) presents indeed negative piezoelectric effect. As already pointed out in the calibration part, also from the analysis of EFM signals came out that the orientation of the hysteresis loops and the values of EFM phase in the PFM images, confirm that P(VDF-TrFE) shows negative piezoelectric effect.

4.3 PFM on P(VDF-TrFE) nanofibers

In this section I will describe the main part of this work, i.e. a microscopic analysis of electrospun PVDF-TrFE nanofibers in order to extend the comprehension of effects on piezo- and ferroelectric properties due to electrospinning and in particular to nanoconfinement.

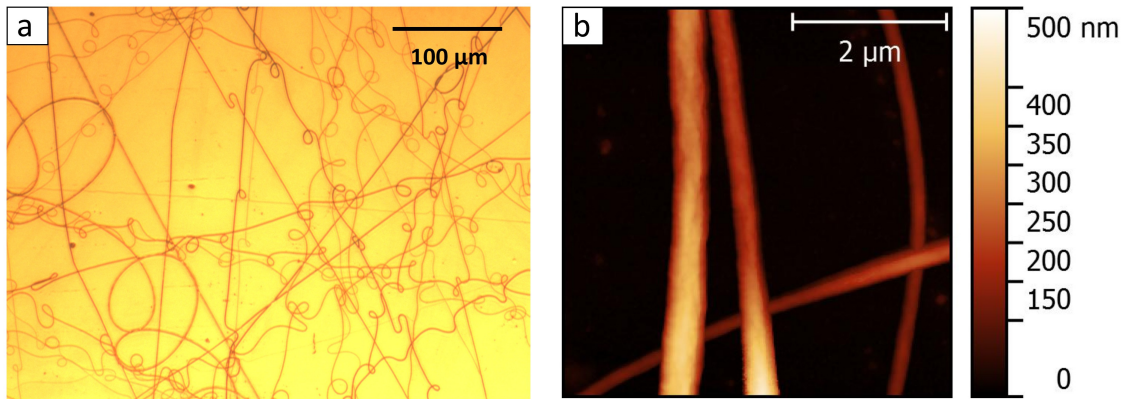


FIGURE 4.8: a) Optical image of electrospun (+20 kV) PVDF-TrFE nanofibers on Au, b) non-contact AFM image of surface morphology that shows more details of nanofibers.

In Figure 4.8 it is presented, with an optical image(a) and a non-contact AFM scan(b), one of the samples examined. As already described in Chapter 2, nanofibers were randomly deposited. In order to investigate the impact of electrospinning conditions on fibers properties, PVDF-TrFE nanofibers were electrospun

applying positive and negative voltage and on different substrates, both conductive (Au and ITO) and insulating (SiO_2/Si). From several height images like the one in Figure 4.8b, one can notice a distribution in dimensions of the fibers that goes from about 100 nm to over 1 μm of diameter independently from substrate and electrospinning potential. The shape and reduced dimensions of nanofibers bring two additional challenges to SS-PFM and PFM measurements. First, for each hysteresis loops characterization I had to accurately position the probe on the center of the fiber, to exclude the possibility of contact between tip and substrate while the SMU was active, avoiding shortcircuits, potentially damaging the AFM tip. Second, being PFM a contact technique, there is the risk to displace the fibers less attached on the substrate with the movement of the scanning probe. However, with some precaution I succeeded in polarization and examination of nanofibers.

In Figure 4.9 are shown the results obtained from the same experiment described in the previous section made on the thin film. First of all from Figure 4.9c, we can observe a mean diameter along the fiber of 470 nm, so I would have expected a coercive potential smaller to the one applied for the polarization of the film's groove. Nevertheless, it was observed on fibers, that there is a sort of initial barrier to induce saturation polarization for the first time, such that I had to apply potential greater than 100 V to achieve the complete reorientation of domains. In fact in the plot one can see how the DC bias applied seems to be higher than necessary, that is because I set a level of DC bias high enough to achieve the first saturation. Once it is reached the saturation, as showed in Figure 4.9a-b) one obtains similar plots of piezoresponse and polarization already shown for the thin film. The graphs displays a coercive potential for the nanofibers of about 70 V, higher than expectation from the results on thin film. The deformation instead, is about 100 pm, similar to the one acquired on thin film.

As for the SS-PFM experiments performed on the the thin film, such levels of voltage lead to the penetration of the tip into the P(VDF-TRFE) fiber leaving holes on the surface (Figure 4.9c). In the case of this specific fiber it was performed two consecutive SS-PFM measurements at a distance of about 1 micron, setting the voltage step function such that, the two spectroscopies ended with opposite voltage sign. As expected, Figure 4.9d-e) shows a net switching in polarization, from upward to downward following the different signs of the poling voltage. The signal extends all over the width of the fiber demonstrating that all the dipoles of PVDF-TrFE were aligned in the direction perpendicular to the fiber axis. Another

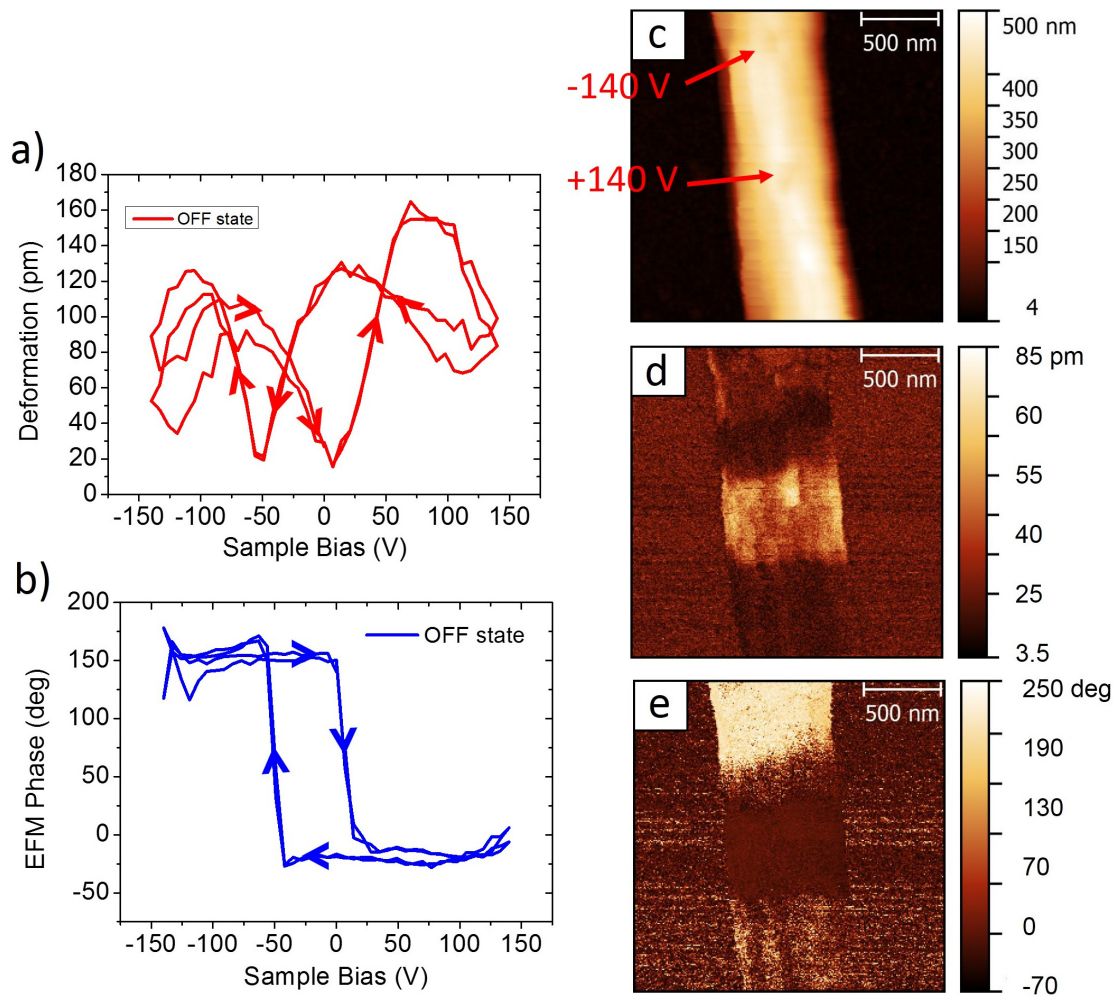


FIGURE 4.9: SS-PFM and PFM scan on a PVDF-TrFE nanofiber deposited on Au substrate with +20 kV, a-b) polarization and piezoresponse hysteresis loops, c-d-e) height, piezoresponse and EFM phase images acquired after two poling processes with opposite voltage, negative in the high part of the fiber and positive in the middle.

interesting feature that one can notice from phase and piezoresponse maps is that on the two poled area, a significant EFM signal is measured, whereas on unpoled areas of the fiber, no significant signal can be revealed. This means that without applying DC potentials to the fibers, polymer's dipoles are initially randomly oriented and there is only small electrostriction response to the alternating electric field generated by the tip. Finally at high levels of applied voltage, instabilities in the EFM signal and a reduction in oscillation amplitude are observed (Figure 4.9a). Although, in Figure 4.9d-e), we can not see clearly the spots left by the tip with

opposite EFM phase signal and higher EFM amplitude as in Figure 4.6d-e), the responsible for the unstable behaviour of EFM amplitude trace, could be the already cited phenomenon of ionization induced nearby the tip.

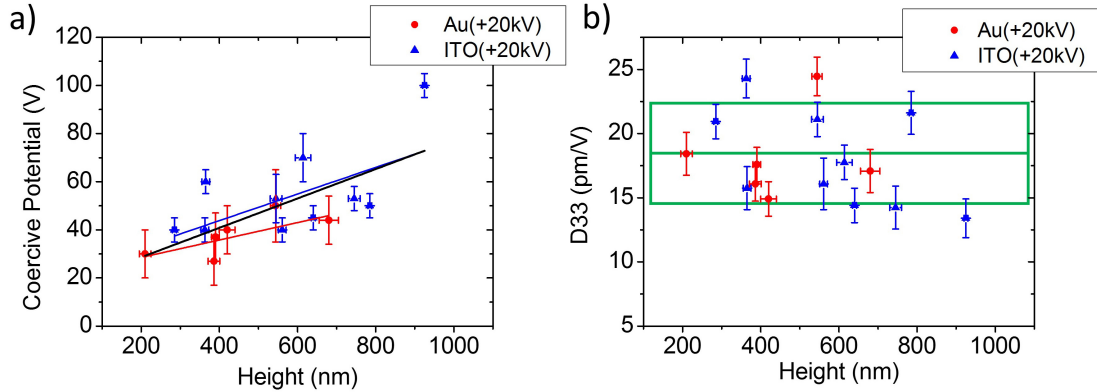


FIGURE 4.10: Relationship between thickness and a) coercive potential, b) d_{33} in PVDF-TrFE nanofibers electrospun on Au and ITO. In the coercive potential plot the lines represent linear fits made on the separate set of data and on all data together (black line), instead in the d_{33} graph, it is reported a mean with his uncertainty relative to the points.

To provide quantitative results I repeated the same measurements illustrated above on fibers with different size, and electrospun at +20 kV on Au and ITO⁴. The variable size of the fibers allowed us to get enough data to study the dependencies between thickness of fibers and the main piezoelectric parameters, d_{33} and coercive potential with comparison between substrates. As we can see in Figure 4.10 there are not real differences of piezoelectric behaviour related to the substrate. Fitting the data reported on the plot in Figure 4.10a, we can estimate a coercive field of (60 ± 10) V/ μm . This estimation is made assuming the system tip, fibers and substrate, as a parallel capacitor. Although this is a massive simplification and the value reported for coercive field may be a little bit underestimated, the result confirms the trend of increasing potential necessary for polarize fibers with growing size. In the thin film the coercive potential goes from 20 V for 100 nm to 80V for 700 nm, suggesting an higher values in V/ μm than the one reported for the fibers. I would take this comparison with caution since we have not lots of data regarding the film and we ca not say with certainty if the dependence between coercive

⁴Unfortunately samples electrospun on Si/SiO₂ were useless for PFM because of the low adhesion of fibers on substrate

potential and height is linear for both film and fibers. In the literature, it has been speculated that nanoconfinement would lead to different and maybe enhanced piezoresponse of PVDF-TrFE nanofibers compared to thin film configuration [37]. For what it was observed, this is not the case, in fact Figure 4.10b shows that, d_{33} is independent from the size of fibers. The mean value of measured piezoelectric strain constant in fibers is $d_{33} = (18 \pm 4)$ pm/V, similar to the one registered in the film. Therefore, we can not state that an improvement of piezoelectric performance is related to the electrospun fibers in the range of size that we have investigated. Finally to explain the not always regular distribution of data, it has to be taken in account that the choice of position on fibers during SS-PFM is crucial for this kind of measure, i.e. piezoelectric properties are strongly dependent by the different grades of crystallinity of PVDF-TrFE along fibers.

4.4 Charging effects in electrospun P(VDF-TrFE) nanofibers

In this last section I will analyse the effects due to electrospinning regarding charging processes or polarization of P(VDF-TrFE) during the deposition. We used the SPM in KPFM mode in order to gain surface potential information from all different samples⁵.

Looking at Figure 4.11a, we can see a 10 micron scan of some fibers electrospun on Au with +20 kV, displaying morphology and surface potential. The height image, shows an apparent variation of thickness along two of the fiber's nearby intersection with other fibers. Actually, this indicates a lift of the structures from the surface, i.e. a separation between the conductive substrate and PVDF-TrFE. The interesting thing that one notices from comparison with the surface potentials image is that in the same zones of separation, there is higher negative surface potentials. Thus, it means that during electrospinning some charges were trapped by the polymer and that the conductive substrate plays a role in the neutralization of this charges. Another confirmation of the charging effect induced by electrospinning came from the measurements on insulating substrates.

Figure 4.11b-c) shows KPFM images of fibers electrospun on SiO₂, applying +20 kV and -20 kV. In this case we can see how the surface potential signals are

⁵Non-contact modes like KPFM does not require good adhesion of the fibers, so there were not problems to perform measurements on insulating substrates.

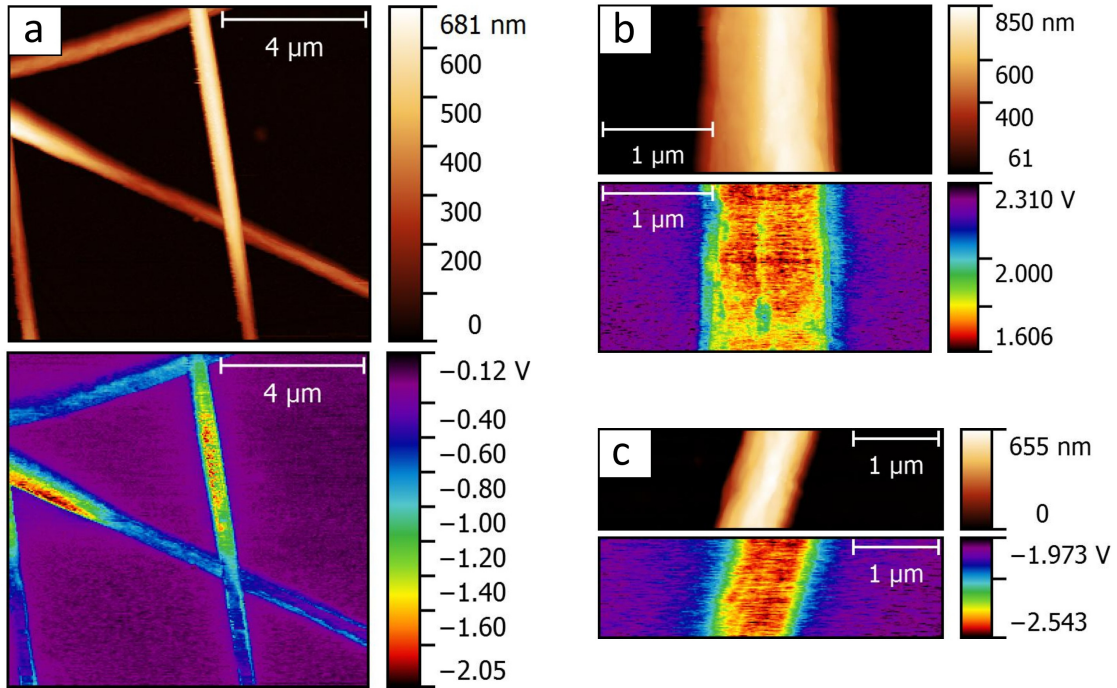


FIGURE 4.11: KPFM non-contact images of height and surface potential taken from different samples. a) $10\ \mu\text{m}$ scan of some electrospun fibers at $+20\ \text{kV}$ on Au substrate, b-c) fiber on Si/SiO₂ substrates electrospun respectively at $+20\ \text{kV}$ and $-20\ \text{kV}$.

higher all over the samples because of the charges deposited and trapped by both insulating substrate and fibers. Furthermore, the difference of surface potential between substrate and fiber is quite similar for the two samples, but the sign of acquired signals is correlated to the electrospinning voltage. Importantly, although the substrate surface is insulating silicon oxide, KPFM measurements are still possible as the surface voltage is referred to the bulk of the substrate material that is highly doped conductive silicon.

Figure 4.12a presents the variation of fibers surface potential measured at different times after the preparation of the samples. The reported data came from thick and regular fibers electrospun on Au and from a simply dropcast PVDF-TrFE on Au. Even though, only few points were acquired, it's clear the decrease of surface potential with passing time. The sample labeled as "thick" was electrospun with an higher concentration of the copolymer that lead to thicker fibers (more than $1\ \mu\text{m}$), so it was useless for SS-PFM measures⁶, but it made me notice a correlation between thickness and initial surface potential (see the red points

⁶Such thicknesses lead to coercive potential too high for execute SS-PFM without damaging the tip.

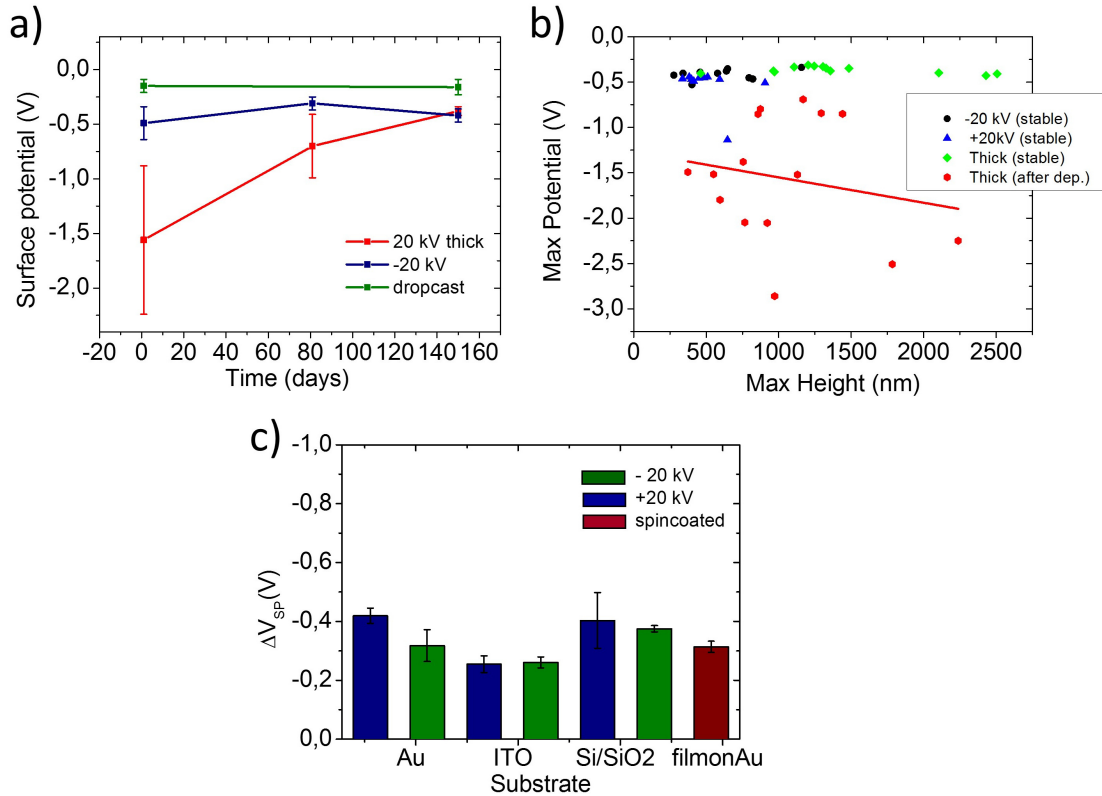


FIGURE 4.12: Comparison on data acquired on different substrate and electrospinning potential. a) surface potential variation at different times after the deposition, b) relationship between fiber's size and surface potential, c) histogram reporting mean values of surface voltage differences between substrates and PVDF-TrFE.

in Figure 4.12b). After some months from the deposition, in every samples with a conductive substrate it was observed the same level of surface potentials (Figure 4.12b). A comparison of mean values of surface potentials, is shown in the histogram of Figure 4.12c. Each value represents the differences of surface potential between PVDF-TrFE and substrate. It can be noticed that even if in the case of SiO₂ I have measured positive and negative surface potential, the relative mean values are all negative and similar to each other. It's not clear the source of the small differences observed between samples, but seems to be more linked to the kind of substrate than to the sign of electrospinning potential.

Considering these information, it seems that $P(\text{VDF-TrFE})$ accumulates charges during the electrospinning process and then behaves like an electret (see Chapter 1), maintaining the charge for a certain period of time. These space charges trapped during electrospinning process are dissipated because of the not zero conductivity

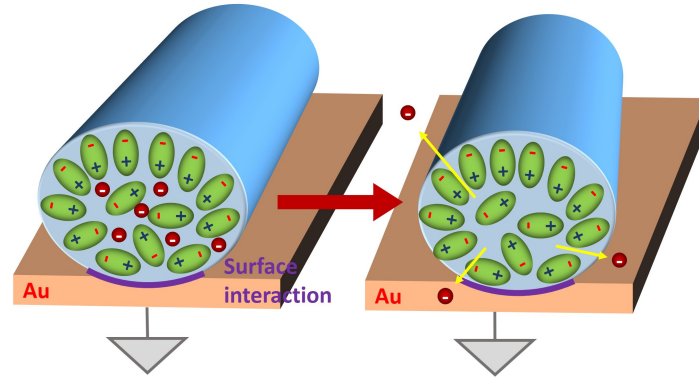


FIGURE 4.13: Schematization of the process responsible for the results acquired with KPFM. Interfacial unbalanced dipoles could explain the observed surface potential.

of P(VDF-TrFE), sufficient to release charges in a relative short time. However, after the dissipation of charges, the surface potential above the fibers remain negative and stable. In addition, also negative surface potentials are observed on films. Hence, the surface potential measured on P(VDF-TrFE) after few months can not be related to the electrospinning process. This charge is also independent of thickness, so it is necessarily related to some interface effect. A global interpretation could be that the initial stronger signal is due to trapped charge, then some substrate interaction, generates an alignment of dipoles that produces the lower surface potential signal. In particular, I think that there's a certain alignment of dipoles in the surface of fibers except for the parts subjected to contact potentials with substrate. This could explain the similar values of surface potentials measured with KPFM and the relationship with the kind of substrate that induce different contact with the polymer (Figure 4.13).

4.4.1 Effects of Polarization Switching on Surface Potential

Figure 4.14e, shows a schematic representation of our last experiment, designed to gain more information about the relation between surface potential and fiber polarization. In order to obtain consecutive neighboring zones with opposite polarization, I used to execute consecutive spectroscopy acquisition ending with both positive and negative step functions. After the polarization process, it was acquired PFM images to check the effective state of polarization along the fiber and to have a comparison with KPFM image that it would be acquired consecutively.

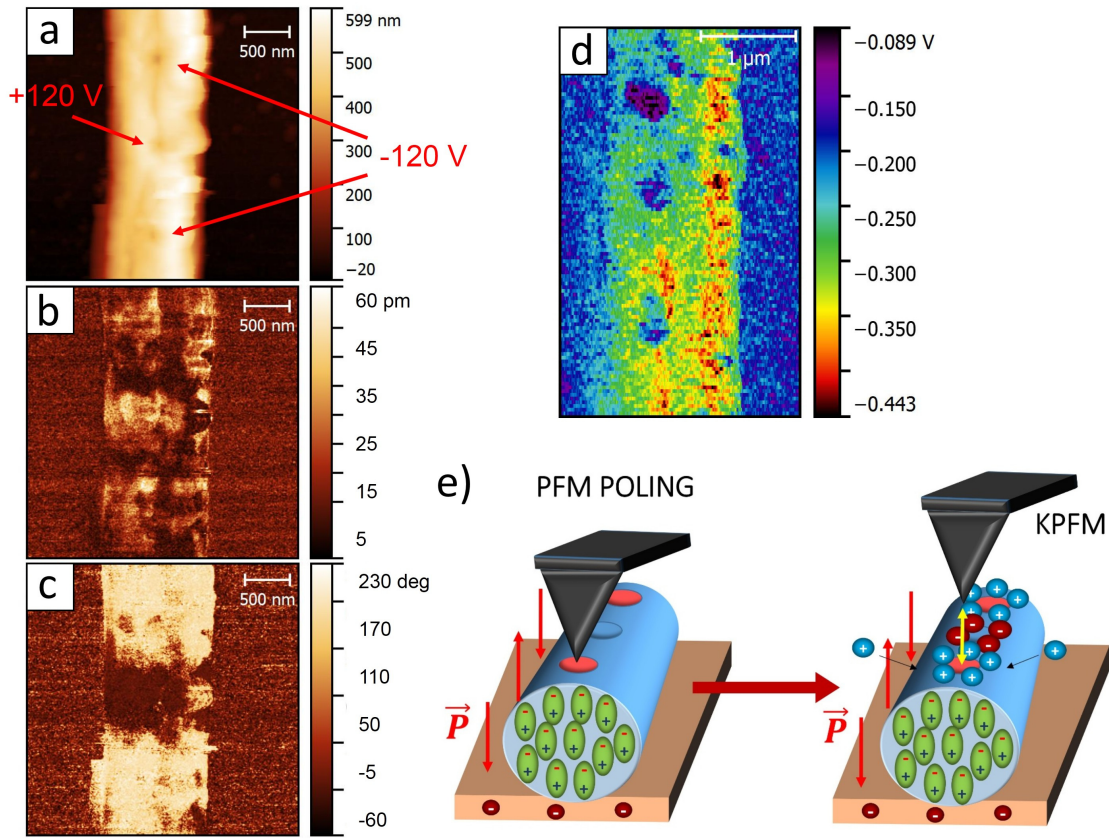


FIGURE 4.14: PFM on fiber electrospun on Au (-20kV) showing a) height, b) piezoresponse and c) polarization after consecutive and opposite poling process (SS-PFM, range ± 120 V) performed on fiber at $1 \mu\text{m}$ of distance to each other. d) Effects on surface potential caused by aligned dipoles. e) Schematization of the experiment, to display the presence of screening effect.

We can see clearly three well separated regions of polarization. From the height image (Figure 4.14a), it can be determined the position of the tip during poling operations. In Figure 4.14b, we can observe the variation of piezoresponse signal that almost disappear where there is a transition of dipoles orientation. The reorientations are shown in the phase image (Figure 4.14c) that represent the change of polarization from upward to downward, polarization that extends just from the positions of tip during SS-PFM. The alignment of PVDF-TrFE dipoles lead also to an accumulation of positive or negative charges nearby the surface of the fiber depending on the poling potential applied. Thus, I would expect a strong KPFM signal due to the polarization of the polymer. Looking at Figure 4.14d, even if we can see some spot with lower negative surface potential, there is not significant difference with respect to the already shown KPFM images. In fact, the difference

of surface potential between substrate and PVDF-TrFE is almost the same that it was reported in Figure 4.12. Since I operated at room condition, this unexpected result came out surely from a screening effect, probably due to ionization of water molecules that are oxidized or reduced at the AFM tip to produce OH^- and H^+ , capable of neutralize the surface potential on the fiber (Figure 4.14e).

Conclusions

Ferroelectric organic materials, like polyvinylidene fluoride (PVDF) and its copolymer with trifluoroethylene (TrFE), have attracted great interest in technological research for the promising potential applications in, biocompatible, flexible and low-cost, modern electronics, such as energy harvesting for self-powered devices, bio-sensors and lead-free FRAM's. At the actual state of the art, P(VDF-TrFE) is the best candidate for development of commercial application, but further studies has to be done in order to improve the material performance.

In this thesis, the effects of electrospinning on ferro- and piezoelectric properties of P(VDF-TrFE) copolymer, have been analyzed at the nanometer scale through different techniques of Scanning Probe Microscopy (PFM, KPFM). A comparison between electrospun nanofibers and a thin film (see Chapter 2) has been presented, in order to have a better comprehension of the effects induced by nanoconfinement and electrospinning charging process.

The lowering in dimension, has been suggested to be one of the most effective way to improve the properties of ferroelectric materials [71]. Furthermore, although P(VDF-TrFE) is the most attractive material for electromechanical applications, the presence of the ferroelectric β -phase is not sufficient to induce piezoelectric character because "poling" is also required in order to align the dipoles of the copolymer [72]. Electrospinning has been suggested to be one of the solution to this problem, inducing polarization in nanofibers during the deposition and avoiding the required post poling process [73, 74].

Combining the results obtained from the experiments with PFM and KPFM, it seems that electrospinning does not induce polarization on the fibers, since PFM images reports no differences in the spontaneous polarization between fibers and the film, which has not been subjected to post poling process. Without the application of external electric fields, the orientation of polarization is randomly distributed along the samples and the piezoresponse signal is absent, proving that there is not poling effect induced by electrospinning. KPFM data reveals that the effect due to electrospinning is instead an accumulation of charges in the nanofibers, since we

observe an initial stronger surface potential signal. These charges are dissipated with passing time, reaching a stable negative level of surface potential.

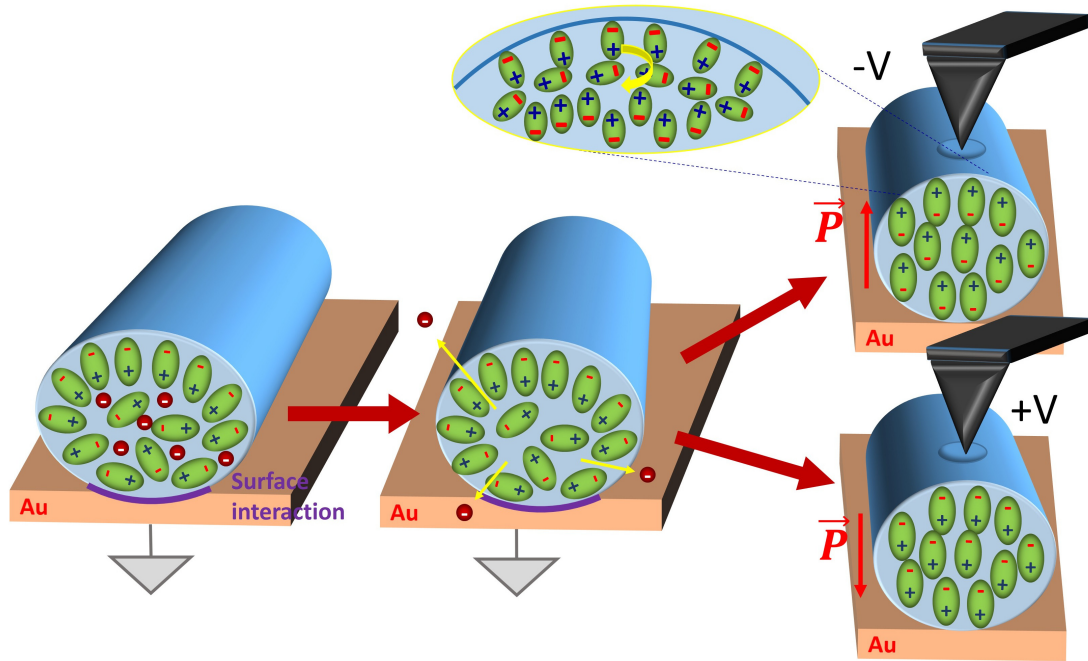


FIGURE 4.15: Schematization of effects and processes induced on PVDF-TrFE nanofibers by electrospinning deposition and our experiments.

These major findings of my thesis are summarized schematically in Figure 4.15. The Figure shows a schematisation of the model developed after the analysis of data brought by the experiments illustrated in Chapter 4. Right after deposition, electrospun P(VDF-TrFE) nanofibers present trapped space charges that could give misleading data in macroscopic experiments, suggesting that the sample is polarized by electrospinning. However, like in electrets, the electric response to mechanical stimuli is caused by the movement of such charges. The contact with conductive substrates lead to a dissipation of the trapped charges, and in a time of the order of few months, a negative surface potential is observed. The same negative potential is measured on the thin film sample, so our hypothesis is that in both cases there has to be an interface effect, such as a contact interaction with the substrate, that results in an unbalanced orientation of dipoles between different interfaces. To be more clear, we suppose that dipoles at the surface are aligned with the negative side neighboring the interface expect for the ones near the substrates that are less aligned, this non-equilibrium between bottom and top of the fibers results in the overall negative surface potential.

Even if we have witnessed that electrospinning does not lead to a defined polarization of deposited nanofibers, it has been shown that is possible to pole and switch the polarization of nanofibers (upward and downward) with the SPM probe, demonstrating the piezoelectric behaviour of this material. Another thing to notice is that the negative layer of surface charges is still present when the polarization points upward, since the surface potential after poling process is always negative. A comparison between values of d_{33} and coercive potentials, reported for the thin film and nanofibers, suggests that there is not a real improvement of performance with lower dimensionality.

In conclusion, electrospun P(VDF-TrFE) nanofibers needs a post poling process in order to be used for energy harvesting application. Furthermore, the coercive field observed is well above the air dielectric breakdown, so to achieve the polarization in films containing electrospun nanofibers, it is clear that nanofibers have to be integrated in a matrix of material with enough dielectric strength to avoid electric discharge during the application of poling field. Once this is achieved, we predict a significant improvement of electromechanical properties.

Bibliography

- [1] I.R. Henderson. “Piezoelectric Ceramics: Principles and Applications”. In: *Pennsylvania: APC International Ltd* (2006).
- [2] Takeo Furukawa. “Ferroelectric properties of vinylidene fluoride copolymers”. In: *Phase Transitions: A Multinational Journal* 18.3-4 (1989), pp. 143–211.
- [3] T Furukawa, Y Takahashi, and T Nakajima. “Recent advances in ferroelectric polymer thin films for memory applications”. In: *Current Applied Physics* 10.1 (2010), e62–e67.
- [4] Ronald CG Naber et al. “Organic nonvolatile memory devices based on ferroelectricity”. In: *Advanced materials* 22.9 (2010), pp. 933–945.
- [5] Pamela Hitscherich et al. “The effect of PVDF-TrFE scaffolds on stem cell derived cardiovascular cells”. In: *Biotechnology and bioengineering* (2016).
- [6] Sam Crossley and Sohini Kar-Narayan. “Energy harvesting performance of piezoelectric ceramic and polymer nanowires”. In: *Nanotechnology* 26.34 (2015), p. 344001.
- [7] Martin Bohlén and Kim Bolton. “Conformational studies of poly (vinylidene fluoride), poly (trifluoroethylene) and poly (vinylidene fluoride-co-trifluoroethylene) using density functional theory”. In: *Physical Chemistry Chemical Physics* 16.25 (2014), pp. 12929–12939.
- [8] Valentina Cauda et al. “Nanoconfinement: an effective way to enhance PVDF piezoelectric properties”. In: *ACS applied materials & interfaces* 5.13 (2013), pp. 6430–6437.
- [9] Dipankar Mandal, Sun Yoon, and Kap Jin Kim. “Origin of Piezoelectricity in an Electrospun Poly (vinylidene fluoride-trifluoroethylene) Nanofiber Web-Based Nanogenerator and Nano-Pressure Sensor”. In: *Macromolecular rapid communications* 32.11 (2011), pp. 831–837.
- [10] Joe Briscoe and Steve Dunn. *Nanostructured Piezoelectric Energy Harvester*. Queen Mary University of London, London, UK: Springer, 2014.

-
- [11] M. S. Vijaya. *Piezoelectric material devices*. 6000 Broken Sound Parkway NW: Taylor and Francis Group, 2013.
- [12] Uchino K. et al. “Electrostrictive effects in non-polar perovskites”. In: *Phase Transitions* 1 (1980), p. 333.
- [13] Zhenyi M. et al. “High field electrostrictive response of polymers”. In: *J. Polym. Sci. B* 32 (1994), p. 2721.
- [14] Jaffe H. and Berlincourt D. A. “Piezoelectric transducer materials”. In: *Proc. IRE* 53 (1965), p. 1372.
- [15] Fei Li et al. “Electrostrictive effect in ferroelectrics: An alternative approach to improve piezoelectricity”. In: *Applied Physics Reviews* 1.1 (2014), p. 011103. URL: <http://dx.doi.org/10.1063/1.4861260>.
- [16] Kiia Tammi. *Piezoelectric Sensing*. URL: <https://wiki.metropolia.fi/display/sensor/Piezoelectric+sensing>.
- [17] S.O. Reza Moheimani and Andrew J. Fleming. *Piezoelectric Transducers for Vibration Control and Damping*. School of Electrical Engineering and Computer Science, University of Newcastle, University Drive, Callaghan, NSW 2308 Australia: Springer, 2006.
- [18] JS Harrison and Zoubeida Ounaies. *Polymers, piezoelectric*. Wiley Online Library, 2002.
- [19] Sergei V Kalinin et al. “Local polarization dynamics in ferroelectric materials”. In: *Reports on Progress in Physics* 73.5 (2010), p. 056502. URL: <http://stacks.iop.org/0034-4885/73/i=5/a=056502>.
- [20] Premi Chandra and Peter B. Littlewood. “A Landau Primer for Ferroelectrics”. In: *Physics of Ferroelectrics: A Modern Perspective*. Berlin, Heidelberg: Springer Berlin Heidelberg, 2007, pp. 69–116. ISBN: 978-3-540-34591-6. DOI: [10.1007/978-3-540-34591-6_3](https://doi.org/10.1007/978-3-540-34591-6_3). URL: http://dx.doi.org/10.1007/978-3-540-34591-6_3.
- [21] O. Heaviside. *Electrical Papers*. Chelsea scientific books v. 1. Macmillan and Company, 1892. URL: <https://books.google.it/books?id=bU7PAAAAMAAJ>.
- [22] G.M. Sessler and M.G. Broadhurst. *Electrets*. Topics in applied physics. Springer-Verlag, 1980. ISBN: 9783540095705. URL: <https://books.google.it/books?id=oLXvAAAAMAAJ>.

- [23] M. Eguchi. In: *Phil. Mag.* 49 (1925), p. 178.
- [24] A. Gemant. In: *Phil. Mag.* 20 (1935), p. 929.
- [25] B. Gross. In: *Phys. Rev.* 66 (1944), p. 26.
- [26] H.S. Nalwa. *Ferroelectric Polymers: Chemistry, Physics, and Applications*. Plastics Engineering. Taylor & Francis, 1995. ISBN: 9780824794682. URL: https://books.google.it/books?id=%5C_M8B6ISHxFUC.
- [27] A. Meissner and R. Bechmann. In: *Z. Tech. Phys* 9 (1928), pp. 174, 430.
- [28] Heiji Kawai. “The Piezoelectricity of Poly (vinylidene Fluoride)”. In: *Japanese Journal of Applied Physics* 8.7 (1969), p. 975. URL: <http://stacks.iop.org/1347-4065/8/i=7/a=975>.
- [29] R. G. Kepler and R. A. Anderson. “Ferroelectricity in Polyvinylidene Fluoride”. In: *J. Appl. Phys.* 9.3 (1978), pp. 1232–1235.
- [30] Qi Li and Qing Wang. “Ferroelectric Polymers and Their Energy-Related Applications”. In: *Macromolecular Chemistry and Physics* 217.11 (2016), pp. 1228–1244. ISSN: 1521-3935. DOI: [10.1002/macp.201500503](https://doi.org/10.1002/macp.201500503). URL: <http://dx.doi.org/10.1002/macp.201500503>.
- [31] Kenji Omote, Hiroji Ohigashi, and Keiko Koga. “Temperature dependence of elastic, dielectric, and piezoelectric properties of “single crystalline” films of vinylidene fluoride trifluoroethylene copolymer”. In: *Journal of Applied Physics* 81.6 (1997), pp. 2760–2769. DOI: [10.1063/1.364300](https://doi.org/10.1063/1.364300). URL: <http://dx.doi.org/10.1063/1.364300>.
- [32] Jodie L. Lutkenhaus et al. “Confinement Effects on Crystallization and Curie Transitions of Poly(vinylidene fluoride-co-trifluoroethylene)”. In: *Macromolecules* 43.8 (2010), pp. 3844–3850. DOI: [10.1021/ma100166a](https://doi.org/10.1021/ma100166a). URL: <http://dx.doi.org/10.1021/ma100166a>.
- [33] Valentina Cauda et al. “Nanoconfinement: an Effective Way to Enhance PVDF Piezoelectric Properties”. In: *ACS Applied Materials & Interfaces* 5.13 (2013), pp. 6430–6437. DOI: [10.1021/am4016878](https://doi.org/10.1021/am4016878). URL: <http://dx.doi.org/10.1021/am4016878>.
- [34] Matthew Poulsen and Stephen Ducharme. “Why ferroelectric polyvinylidene fluoride is special”. In: *IEEE Transactions on Dielectrics and Electrical Insulation* 17.4 (2010).

- [35] S Palto et al. “Ferroelectric langmuir-blodgett films”. In: *Ferroelectrics Letters Section* 19.3-4 (1995), pp. 65–68.
- [36] Manfang Mai et al. “Ferroelectric Polymer Thin Films for Organic Electronics”. In: *Journal of Nanomaterials* 2015 (2015), p. 14. DOI: [10.1155/2015/812538](https://doi.org/10.1155/2015/812538).
- [37] Longyue Liang et al. “One-Dimensional Ferroelectric Nanostructures: Synthesis, Properties, and Applications”. In: *Advanced Science* 3.7 (2016), 1500358–n/a. DOI: [10.1002/advs.201500358](https://doi.org/10.1002/advs.201500358). URL: <http://dx.doi.org/10.1002/advs.201500358>.
- [38] Canan Dagdeviren et al. “Recent progress in flexible and stretchable piezoelectric devices for mechanical energy harvesting, sensing and actuation”. In: *Extreme Mechanics Letters* 9, Part 1 (2016), pp. 269–281. DOI: <http://dx.doi.org/10.1016/j.eml.2016.05.015>. URL: <http://www.sciencedirect.com/science/article/pii/S2352431616301092>.
- [39] Xiaoliang Chen et al. “A high performance P(VDF-TrFE) nanogenerator with self-connected and vertically integrated fibers by patterned EHD pulling”. In: *Nanoscale* 7 (27 2015), pp. 11536–11544. DOI: [10.1039/C5NR01746G](https://doi.org/10.1039/C5NR01746G). URL: <http://dx.doi.org/10.1039/C5NR01746G>.
- [40] Feng Ru Fan, Wei Tang, and Zhong Lin Wang. “Flexible Nanogenerators for Energy Harvesting and Self-Powered Electronics”. In: *Advanced Materials* 28.22 (2016), pp. 4283–4305. ISSN: 1521-4095. DOI: [10.1002/adma.201504299](https://doi.org/10.1002/adma.201504299). URL: <http://dx.doi.org/10.1002/adma.201504299>.
- [41] N. H. Van et al. In: *Nano-Micro Lett.* 7.35 (2015).
- [42] T. J. Reece et al. “Nonvolatile memory element based on a ferroelectric polymer Langmuir-Blodgett film”. In: *Applied Physics Letters* 82.1 (2003), pp. 142–144.
- [43] G. A. Salvatore, D. Bouvet, and A. M. Ionescu. “Demonstration of subthreshold swing smaller than 60mV/decade in Fe-FET with P(VDF-TrFE)/SiO₂ gate stack”. In: *2008 IEEE International Electron Devices Meeting*. Dec. 2008, pp. 1–4. DOI: [10.1109/IEDM.2008.4796642](https://doi.org/10.1109/IEDM.2008.4796642).
- [44] Y. Yuan, T. J. Reece, and P. et al. Sharma. “Efficiency enhancement in organic solar cells with ferroelectric polymers”. In: *Nature Materials* 10.4 (2011), pp. 296–302.

- [45] S. Salahuddin and S. Datta. “Use of negative capacitance to provide voltage amplification for low power nanoscale devices”. In: *Nano Letters* 8.2 (2008), pp. 405–410.
- [46] Thomas Lenz et al. “Microstructured organic ferroelectric thin film capacitors by solution micromolding”. In: *physica status solidi (a)* 212.10 (2015), pp. 2124–2132.
- [47] Marco Zaccaria. “Electrospun materials for energy applications: from Lithium-ion batteries to electrets”. Tesi di Dottorato. Università di Bologna, 2016.
- [48] Oxolutia. *Electrospinning*. URL: <http://www.oxolutia.com/technology/electrospinning/>.
- [49] P Schümmer and KH Tebel. “A new elongational rheometer for polymer solutions”. In: *Journal of Non-Newtonian Fluid Mechanics* 12.3 (1983), pp. 331–347.
- [50] Teeradech Jarusuwannapoom et al. “Effect of solvents on electro-spinnability of polystyrene solutions and morphological appearance of resulting electro-spun polystyrene fibers”. In: *European Polymer Journal* 41.3 (2005), pp. 409–421.
- [51] Ladawan Wannatong, Anuvat Sirivat, and Pitt Supaphol. “Effects of solvents on electrospun polymeric fibers: preliminary study on polystyrene”. In: *Polymer International* 53.11 (2004), pp. 1851–1859.
- [52] Peter K Baumgarten. “Electrostatic spinning of acrylic microfibers”. In: *Journal of colloid and interface science* 36.1 (1971), pp. 71–79.
- [53] Shengli Zhao et al. “Electrostatically generated fibers of ethyl-cyanoethyl cellulose”. In: *Cellulose* 10.4 (2003), pp. 405–409.
- [54] Xinhua Zong et al. “Structure and process relationship of electrospun bioabsorbable nanofiber membranes”. In: *Polymer* 43.16 (2002), pp. 4403–4412.
- [55] Shengli Zhao et al. “Electrospinning of ethyl–cyanoethyl cellulose/tetrahydrofuran solutions”. In: *Journal of Applied Polymer Science* 91.1 (2004), pp. 242–246.
- [56] Marin Alexe and Alexei Gruverman. *Nanoscale Characterisation of Ferroelectric Materials, Scanning Probe Microscopy Approach*. 1. Springer-Verlag Berlin Heidelberg, 2004.

- [57] Sergei V. Kalinin and Alexei Gruverman. *Scanning Probe Microscopy, Electrical and Electromechanical Phenomena at the Nanoscale*. 1. Springer-Verlag New York, 2007.
- [58] Sergei V. Kalinin and Alexei Gruverman. *Scanning Probe Microscopy of Functional Materials, Nanoscale Imaging and Spectroscopy*. 1. Springer-Verlag New York, 2011.
- [59] Park System. *AFM NX10*. URL: <https://wiki.metropolia.fi/display/sensor/Piezoelectric+sensing>.
- [60] Asylum Research. *PFM technique*. URL: <https://www.asylumresearch.com/Applications/PFMAppNote/PFMAppNote.shtml>.
- [61] Catherine Dubourdieu et al. “Switching of ferroelectric polarization in epitaxial BaTiO₃ films on silicon without a conducting bottom electrode”. In: *Nature Nanotechnology* 8.10 (2013), pp. 748–754.
- [62] Qi Zhang, Nagarajan Valanoor, and Owen Standard. “Chemical solution deposition derived (001)-oriented epitaxial BiFeO₃ thin films with robust ferroelectric properties using stoichiometric precursors (invited)”. In: *Journal of Applied Physics* 116.6 (2014), p. 066810. DOI: [10.1063/1.4891311](https://doi.org/10.1063/1.4891311). URL: <http://dx.doi.org/10.1063/1.4891311>.
- [63] Oxford Instruments. URL: [https://www.oxford-instruments.com/businesses/nanotechnology/asylum-research/gallery/piezoresponse-force-microscopy-\(pfm\)](https://www.oxford-instruments.com/businesses/nanotechnology/asylum-research/gallery/piezoresponse-force-microscopy-(pfm)).
- [64] M Nonnenmacher, MP o’Boyle, and H Kumar Wickramasinghe. “Kelvin probe force microscopy”. In: *Applied physics letters* 58.25 (1991), pp. 2921–2923.
- [65] Wilhelm Melitz et al. “Kelvin probe force microscopy and its application”. In: *Surface Science Reports* 66.1 (2011), pp. 1–27.
- [66] R. Garcia and R. Perez. In: *Surface Science Reports* 47 (2002), p. 197.
- [67] F.J. Giessibl. In: *Rev. Modern Phys.* 75 (2003), p. 949.
- [68] T.R. Albrecht et al. In: *Journal of Applied Physics* 69 (1991), p. 668.
- [69] Vladimir S Bystrov et al. “Molecular modeling of the piezoelectric effect in the ferroelectric polymer poly (vinylidene fluoride)(PVDF)”. In: *Journal of molecular modeling* 19.9 (2013), pp. 3591–3602.

-
- [70] Ilias Katsouras et al. “The negative piezoelectric effect of the ferroelectric polymer poly(vinylidene fluoride)”. In: *Nature Materials* 15.1 (2016), pp. 78–84.
- [71] Justin Varghese, Roger W Whatmore, and Justin D Holmes. “Ferroelectric nanoparticles, wires and tubes: synthesis, characterisation and applications”. In: *Journal of Materials Chemistry C* 1.15 (2013), pp. 2618–2638.
- [72] Valentina Cauda, Giancarlo Canavese, and Stefano Stassi. “Nanostructured piezoelectric polymers”. In: *Journal of Applied Polymer Science* 132.13 (2015).
- [73] Vitor Sencadas et al. “Local piezoelectric response of single poly (vinylidene fluoride) electrospun fibers”. In: *physica status solidi (a)* 209.12 (2012), pp. 2605–2609.
- [74] Luana Persano et al. “High performance piezoelectric devices based on aligned arrays of nanofibers of poly (vinylidene fluoride-co-trifluoroethylene)”. In: *Nature communications* 4 (2013), p. 1633.